Naval Research Laboratory

Washington, DC 20375-5000

NRL Memorandum Report 6884

Numerical Simulations of Detonation Transmission

ELAINE S. ORAN

Laboratory for Computational Physics and Fluid Dynamics

DAVID A. JONES

Materials Research Laboratory, D.S.T.O.
P.O. Box 50, Ascot Vale
Victoria, Australia 3032

MARTIN SICHEL

Department of Aerospace Engineering
University of Michigan
Ann Arbor, MI 48109-2140

September 3, 1991

REPORT DOCUMENTATION PAGE

Form Approved
OMB No. 0704-0188

1. AGENCY USE ONLY *(Leave blank)*	2. REPORT DATE	3. REPORT TYPE AND DATES COVERED
	1991 September 3	Interim

4. TITLE AND SUBTITLE

Numerical Simulations of Detonation Transmission

5. FUNDING NUMBERS

PE — 61153N
PR — 44-1527
TA — RR011-09-43
WU — 1527

6. AUTHOR(S)

Elaine S. Oran, David A. Jones* and Martin Sichel**

7. PERFORMING ORGANIZATION NAME(S) AND ADDRESS(ES)

Naval Research Laboratory
Washington DC 20375-5000

8. PERFORMING ORGANIZATION REPORT NUMBER

NRL Memorandum Report 6884

9. SPONSORING/MONITORING AGENCY NAME(S) AND ADDRESS(ES)

Office of Naval Research
U.S. Army Research Office
800 N. Quincy Street
Arlington, VA 22217-5999

10. SPONSORING/MONITORING AGENCY REPORT NUMBER

11. SUPPLEMENTARY NOTES

*Materials Research Laboratory, P.O. Box 50, Ascot Vale, Victoria, Australia 3032
**Department of Aerospace Engineering, University of Michigan, Ann Arbor, MI 48109-2140

12a. DISTRIBUTION/AVAILABILITY STATEMENT

Approved for public release; distribution unlimited.

12b. DISTRIBUTION CODE

13. ABSTRACT *(Maximum 200 words)*

The complex, dynamic shock-detonation structure formed by the glancing interaction of a primary detonation with a secondary explosive is studied using time-dependent two-dimensional simulations and related experiments. The materials considered in the simulations are stoichiometric and lean mixtures of hydrogen and oxygen diluted with argon. Related experiments have used undiluted hydrogen and oxygen as well as other gases. The conditions simulated are a) the primary mixture is stoichiometric and the secondary inert, b) both the primary and secondary mixtures are the same and stoichiometric, c) the primary mixture is lean and the secondary is stoichiometric, and d) the primary mixture is stoichiometric and the secondary is lean. In addition, for cases b) and d), comparisons are made between simulations in which the primary mixture is overdriven and when it is a Chapman-Jouguet detonation. For the overdriven stoichiometric primary detonation interacting with the lean mixture, a complex detonation structure forms and quickly asymptotes to the detonation velocity of the primary mixture. For the same case, but when the primary detonation is initially at Chapman-Jouguet velocity, the detonation appears to die but then reignites due to a series of shock reflections and then propagates as a complex structure. The lowest velocity of the complex structure is always greater than the Chapman-Jouguet velocity of the lean mixture and it increases in time, appearing to approach the Chapman-Jouguet velocity of the stoichiometric mixture. The dynamics of the decay of reignition process are described and discussed in detail.

14. SUBJECT TERMS	15. NUMBER OF PAGES
Shock-detonation structure, Chapman-Jouguet velocity	50
	16. PRICE CODE

17. SECURITY CLASSIFICATION OF REPORT	18. SECURITY CLASSIFICATION OF THIS PAGE	19. SECURITY CLASSIFICATION OF ABSTRACT	20. LIMITATION OF ABSTRACT
UNCLASSIFIED	UNCLASSIFIED	UNCLASSIFIED	

CONTENTS

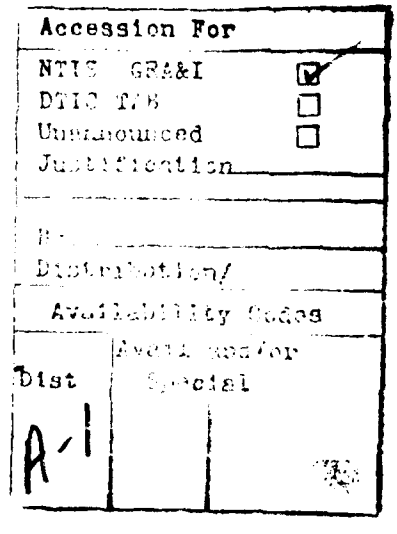

NUMERICAL SIMULATIONS OF DETONATION TRANSMISSION

1. INTRODUCTION

The interaction between a propagating detonation and a bounding energetic medium can have a significant influence both on the detonation itself and on the way energy is transmitted into the bounding medium. When a detonation propagating through the primary explosive first comes into contact with the bounding or secondary explosive, there is an initial transient phase during which the basic interaction pattern becomes established. After that, there are a number of possible types of structures that can form in the bounding material, the exact nature of which depends on the specific properties of the two materials as well as on the degree of overdrive of the incident detonation. Figure 1, a schematic of a detonation propagating through a layered material, shows the blast wave transmitted into the bounding medium (the explosive bubble) and two of the simpler possibilities for subsequent structures: an oblique detonation with Mach reflection from the lower wall and an oblique shock with regular reflection.

This type of interaction is a component of a number of very different types of problems. In the case of gas-phase explosives, the interface between the primary detonation products and the secondary explosive acts as a high-speed gaseous wedge that can induce an oblique detonation in the secondary explosive, as shown on the far right of Figure 1. Such oblique detonations are the basis of the oblique-detonation ramjet engine that has been proposed as a supersonic combustion propulsion system [Sheng and Sislian 1985], and also are a fundamental component of detonation-driven hypervelocity accelerators [Hertzberg et al. 1988]. It is also likely that reactive shock, detonation waves, and wave interactions similar to those observed in layered detonations will arise in supersonic propulsion systems such as the supersonic combustion ramjet.

For detonations in layered condensed explosives, the bounding medium generally has properties different from those of the primary explosive. An important practical question in the design and use of layered explosives is whether a suitable combination of explosives can enhance the effectiveness of the energy transmission compared to using a pure explosive with the same total energy. If the primary and bounding explosives are identical, the layered detonation pattern represents the diffraction that occurs when a detonation propagates past a step or an increase in cross-sectional area, a problem that also has been considered by Bartlma and Schröder [1986]. If the wall of the upper shock tube is considered as an axis of symmetry, the layered detonation also can represent

Manuscript approved June 25, 1991.

the propagation of a detonation from a smaller into a larger tube and then, as indicated by Matsui and Lee [1979], the diameter of the smaller tube must exceed a certain critical value if a detonation is to be initiated in the larger tube. This type of interaction also shows the effects of the presence of a lower reflecting wall on the critical detonation diameter. If the wall of the lower channel is considered the axis of symmetry, the layered detonation simulates an inner explosive sheathed in an outer or primary explosive.

In order to observe experimentally the complex interactions between detonating layers of adjacent explosives, a special double-layer shock-tube was developed and a series of experiments were performed using various combinations of energetic and nonreactive gases in the upper and lower layers [Liu et al. 1987, 1988]. High-speed Schlieren framing photographs were used to record the details of the interaction process, pressure switches monitored the velocity of the primary detonation, and two pressure transducers mounted on the top and bottom walls of the tube recorded the pressure history in each channel. The first analyses of these experiments, using the theory of oblique shock and detonation polars [Liu et al. 1988, Liou 1986, Fan et al. 1988], described a number of possible final steady state shock and detonation configurations. The case in which the bounding gas is inert, first considered by Dabora et al. [1965], showed that an oblique or detached shock is generated in the bounding mixture. When the bounding gas is an explosive, there are a number of possible configurations, two of which are a transmitted oblique shock, or oblique detonation if the primary detonation is sufficiently strong. The theory also showed that other types of interactions are possible [Liou 1986]. Dabora et al. [1991] also performed both experiments and shock-polar studies for the case in which the bounding mixture is an explosive.

The experimental studies revealed that the actual detonation transmission process is often dominated by an initial unsteady refraction process that cannot be described by a shock-polar analysis. Often it is this process which seems to determine the nature of the final steady state configuration. More recently, we have begun to compare these experiments and theoretical predictions to the results of detailed time-dependent numerical simulations [Jones et al. 1991a, Sichel et al. 1990]. The power of the simulations is that for the problem solved, they give basic physical quantities, such as densities, momenta, and energy, and thus any other quantities derived from these, as a function of time and position. The difficulty, however, lies in analyzing the quantity of data produced and in relating the problem actually solved, as determined by the numerical method and the initial conditions, to the actual physical experiment, as determined by the experimental apparatus and experimentally imposed initial conditions.

In this paper, we first summarize the results of the numerical simulations and compare them to related experimental Schlieren framing photographs. The calculations modeled the layered detonations by solving the compressible two-dimensional unsteady equations for a chemically reactive flow, and then the resulting interaction patterns were compared to those observed for gaseous explosives under similar conditions. Direct quantitative comparisons, however, are not yet possible at this stage because the H_2-O_2 mixtures considered in the simulation were diluted with argon while the experiments were conducted using undiluted mixtures. However, the point of describing and comparing simulations and related experiments here is to help understand the resulting complex detonation structure that arises in different cases. The simulations do reproduce the main interaction configurations observed in the experiments and give some confidence that the numerical results are predicting the correct general structures. Then we describe the results of one particularly interesting simulation of the interaction which occurs when a Chapman-Jouguet (CJ) detonation, propagating through a stoichiometric gaseous fuel-oxidizer mixture, comes into contact with a bounding leaner mixture of the same explosive.

In previous simulations, a strong blast wave was used to initiate the primary detonation so that the transmitted detonation was initially overdriven [Jones et al. 1991a]. The result, depending on the explosive mixtures considered, was that either the detonation failed or a steady interaction pattern was rapidly established in the bounding mixture. The final wave structures obtained in these simulations were in qualitative agreement with those observed in experiments conducted in undiluted mixtures of the same explosive where the primary detonation was CJ.

Further computations were then performed in which the same diluted mixtures were used, but the primary detonation was approximately a CJ detonation and not significantly overdriven. In some cases, these results were somewhat different from those obtained for overdriven primary detonations. As already mentioned, the case where the primary detonation is stoichiometric and the secondary mixture is dilute is of particular interest. When the primary detonation was overdriven, the secondary mixture ignited quickly and the final result was a complex, coupled detonation structure moving at the CJ velocity of the primary material. When the primary detonation was at the CJ velocity and not overdriven, the primary detonation initially decayed and appeared to die. Finally, due to the interaction in a double Mach stem that formed after shock reflection, the secondary mixture ignited, the primary mixture reignited, and then the resulting configuration

propagated as an extremely complex, dynamic structure, perhaps on the brink of death, but not dying. By the time the simulation was stopped, this detonation complex had accelerated to a velocity intermediate between the CJ velocity of the two mixtures and was continuing to accelerate.

2. THE MODEL AND METHOD OF SOLUTION

Numerical simulations of gas-phase detonations are based on solutions of the compressible, time-dependent, conservation equations for total mass density ρ, momentum $\rho\mathbf{v}$, and energy E,

$$\frac{\partial \rho}{\partial t} = -\nabla \cdot \rho\mathbf{v} \,, \tag{1}$$

$$\frac{\partial \rho\mathbf{v}}{\partial t} = -\nabla \cdot (\rho\mathbf{v}\mathbf{v}) - \nabla P \,, \tag{2}$$

$$\frac{\partial E}{\partial t} = -\nabla \cdot (E\mathbf{v}) - \nabla \cdot (\mathbf{v}P) \,, \tag{3}$$

where $\mathbf{v}$ is the fluid velocity and P the pressure. In a multispecies fluid in which chemical reactions result in transformations among the species, we also need individual species number densities $\{n_i\}$,

$$\frac{\partial n_i}{\partial t} = -\nabla \cdot n_i\mathbf{v} + Q_i - L_i n_i \,, \qquad i = 1, ..., N_s \,, \tag{4}$$

where the $\{Q_i\}$ and $\{L_i\}$ are chemical production and loss terms, respectively, for species i. The effects of molecular diffusion, thermal conduction, and radiative diffusion have been omitted from these equations. The first two of these effects are generally insignificant on the time scales of interest for detonations and the last is not significant for the hydrogen-oxygen systems of interest here. There is a constraint that defines the total number density N,

$$N = \sum_{i=1}^{N_s} n_i \,, \tag{5}$$

where N_s is the total number of different kinds of species present. The total energy E per unit volume is a sum of the kinetic and internal energy,

$$E = \frac{1}{2}\rho\mathbf{v} \cdot \mathbf{v} + \rho\epsilon \,, \tag{6}$$

where ϵ is the specific internal energy.

An ideal-gas equation of state is used for the gas-phase calculations,

$$P = NkT = \rho RT \,. \tag{7}$$

Also, we assume

$$\rho\epsilon \;=\; \sum_i \rho_i h_i - P \;=\; \rho h - P \tag{8}$$

$$h_i \;=\; h_{io} + \int_{T_o}^{T} c_{pi}\, dT \;, \tag{9}$$

so that the properties of the individual species are taken into account. Here, k is Boltzmann's constant, $\{h_i\}$ the enthalpies of each species i, $\{h_{io}\}$ the heats of formation, and $\{c_{pi}\}$ the specific heats.

In all of the calculations described here, the full set of elementary chemical reactions, that is, the complete set of $\{Q_i\}$ and $\{L_i\}$ describing the elementary reactions, are not included in the model. Instead, we use the induction parameter model that reproduces the essential features of the chemical reaction and energy release process. In the earliest form of this model, three quantities are tabulated as a function of temperature, pressure, and stoichiometry: the chemical induction time, the time during which energy release actually takes place, and the amount of energy released. These quantities may be obtained by integrating the full set of elementary chemical reactions, as we have done for hydrogen-oxygen combustion in this paper, or they may be gathered from experimental data, as we have done previously for liquid nitromethane. Then a quantity called the induction parameter is defined and convected with the fluid in a Lagrangian manner. This parameter records the temperature history of a fluid element and, when the element is heated long enough, energy release is initiated. Such a model works because it reproduces the temperature dependence of the chemical reactions. It is valid as long as the computational timestep is smaller than any of the important fluid-dynamic fluctuations and for fast flows in which the convective timescales are significantly faster than those for physical diffusion. The model was described by Oran et al. [1981] and has been developed further by Kailasanath et al. [1985] and Guirguis et al. [1986, 1987] for studies of the cellular structure of detonations. A similar approach was used for hydrogen combustion by Korobienikov et al. [1981] and Taki and Fujiwara [1976], by Kaplan and Oran [1990] for propane combustion, and by Gubin and Sichel [1977] to model ignition delay in vaporized sprays.

Here the induction parameter model is formulated in a slightly different way than first proposed. We consider two materials: the gas in the upper tube or primary explosive and the gas in the lower tube or secondary explosive, designated by subscripts 1 and 2, respectively. Then the total density

ρ is the sum of the densities,

$$\rho = \rho_1 + \rho_2 \,. \tag{10}$$

The two gases are initially separated in the upper and lower detonation tubes but subsequently come into contact as the detonation in the upper tube encounters the end of the dividing barrier. The chemical transformations that can occur in each gas or mixture of gases proceed by a two-step process that models the full details of the interactions among the species. The first describes the chemical induction period, which is the time during which the reactants break up, intermediate radicals are formed, but there is not yet any substantial energy release so that the mixture remains essentially thermoneutral. Many gases, and in particular hydrogen-oxygen mixtures, have well defined chemical induction times. Energy release occurs in the second step and is a time of rapid reactions and formation of stable products. In hydrogen-oxygen mixtures, this is the time when intermediates such as atomic hydrogen, atomic oxygen, and hydroxyl radicals peak and the product water is formed. In many gases, these two times are not so distinct or there are a number of intermediate or even endothermic stages. The reaction mechanism for hydrogen-oxygen gases, however, can be characterized appropriately by these two times [Burks and Oran 1981], and in this sense the present model is similar to that used by Korobienikov et al. [1972]. It differs from Korobienikov's model, however, in the way the input is derived and therefore in the level of approximation in some regimes of temperature and pressure.

The time corresponding to the first step, the chemical induction period τ^o, is fit to an expression of the form

$$\tau^o = A_\tau \left(\frac{P_o}{P}\right) \exp\left(\frac{E_\tau}{RT}\right) . \tag{11}$$

Then the quantity f, denoting the fraction of the chemical induction time elapsed at time t, may be found from

$$\frac{df}{dt} = \frac{1}{\tau^o(T,P)} \,. \tag{12}$$

In the second step, these reactants are converted to products according to the finite reaction rate

$$\frac{d\omega_i}{dt} = -\omega_i A_r \exp\left(-\frac{E_r}{RT}\right) , \tag{13}$$

where ω_i is the mass fraction of the reactant for each material. The constants A_τ, E_τ, A_r, and E_r are determined from integrating the full set of chemical reaction equations for each material. These constants, τ^o, and the the variables ω and f should all be written with the subscript i referring to the specific material.

The temperature and pressure in a computational cell are given by

$$P = \left(\frac{\eta_1}{m_1} + \frac{\eta_2}{m_2}\right) \rho R_o T \tag{14}$$

and

$$T = \frac{e - \eta_1 \omega_1 \Delta E_1 - \eta_2 \omega_2 \Delta E_2}{\eta_1 C_{v1} + \eta_2 C_{v2}} \tag{15}$$

where η_i is the number-density fraction of species i in a computational cell and ΔE_i, C_{v_i}, and m_i are the energy release, specific heat, and molecular weight for species i.

In a moving system, the time derivatives in Eqs. (12) and (13) indicate a substantial derivative following a fluid particle as it moves through the system. When combined with the continuity equation for each species, they can be rewritten in the same form as Eqs. (1) - (4), that is,

$$\frac{\partial(\rho \omega_i)}{\partial t} + \nabla \cdot (\rho \omega_i \mathbf{v}) = -\rho \omega_i A_{ri} \exp\left(-\frac{E_{ri}}{RT}\right) , \tag{16}$$

$$\frac{\partial(\rho f_i)}{\partial t} + \nabla \cdot (\rho f_i \mathbf{v}) = \frac{\rho_i}{\tau_i^o} \tag{17}$$

for each mixture i. These equations effectively replace Eq. (4).

The convective transport equations, those parts of Equations (1)–(4) (or in this case, Eqs. (16) and (17)) excluding the chemical reaction terms, are solved using the nonlinear, fully compressible flux-corrected transport (FCT) algorithm [Boris and Book 1976, Oran and Boris 1987]. The FCT algorithm is an explicit, conservative, finite-volume method designed to insure that all conserved quantities remain monotonic and positive. It is particularly effective in maintaining steep gradients and generally accurate solutions in both supersonic and subsonic flow calculations. The procedure for using this one-dimensional algorithm with direction and timestep splitting to produce two-dimensional or three-dimensional solutions as well as a number of related calculations performed with it are described in some detail by Oran and Boris [1987]. Specific applications to detonations are described in references such as Jones et al. [1991a], Oran et al. [1981], Kailasanath et al. [1985], Guirguis et al. [1986], and Oran et al. [1988].

Then those parts of the coupled set of equations that describe the chemical reactions, the ordinary differential equations, are solved separately. The equation

$$\frac{d(\rho \omega_i)}{dt} = -\rho \omega_i A_{ri} \exp\left(-\frac{E_{ri}}{RT}\right) \tag{18}$$

is solved implicitly and the equation

$$\frac{d(\rho f_i)}{dt} = \frac{\rho_i}{\tau_i^o} \tag{19}$$

is solved explicitly. These results are combined with the FCT solutions for convective transport by time-step splitting methods, as discussed by Oran and Boris [1987].

3. THE PHYSICAL PROBLEM

The computations model the interaction between two gases: a stoichiometric mixture of hydrogen and oxygen diluted with argon (H_2:O_2:Ar/2:1:7) and a lean mixture of hydrogen and oxygen also diluted with argon (H_2:O_2:Ar/0.5:1:7). The schematic diagram of the computational domain, Figure 2, shows that the primary detonation tube rests on top of the secondary (or bounding) detonation tube. The tubes are separated from each other by a solid barrier that exists until the position 4.0 cm, when the upper and lower tubes come in contact. The physical dimensions shown in the schematic correspond to the experimental apparatus used by Liu et al. [1987, 1988]. The gases are all initially at 1 atm and 298 K.

The properties of the mixtures and the detonations they support were calculated from one-dimensional computations in which a fixed amount of energy was deposited near the origin in the form of excess temperature and pressure. The result of such computations is an overdriven detonation which, in time, decays to CJ conditions. After running such a computation for 20,000 time steps, the detonation velocity was essentially constant. The CJ velocities of the primary and secondary mixtures were 1560 m/s and 1000 m/s, respectively. The detonation cell sizes for these mixtures are 0.1 cm and 0.5 cm, respectively, as estimated from data from Strehlow [Strehlow 1984] for three-dimensional detonations. (For two-dimensional, planar detonations, we would expect the cell sizes to be somewhat different.)

Parameters in the model are chosen so that the detonation has the CJ velocity corresponding to the mixture modeled. The energy release for the primary and secondary mixtures was 0.180 kcal/g and 0.070 kcal/g, respectively, and the molecular weights were 31.6 and 60.0 amu. Values for the reaction parameters A_r, E_r, A_τ, and E_τ are 2.4×10^8 s^{-1}, 3.0×10^4 kcal, $5.6840 \times 10^{-8} s^{-1}$, and 1.5031×10^4 kcal, respectively, for both mixtures. In addition, the value of γ is held constant in the calculation: it is not allowed to be a function of composition or temperature. This is certainly an unphysical assumption. Here, however, this is part of the simplified parametric model that ensures that the values of certain global physical quantities, such as the detonation velocity, have

the correct physical value. Selecting and fitting these parameters must be viewed in the same way and are at the same level of approximation as the induction parameter model.

The simulations were carried out on an evenly spaced rectangular grid with $\Delta x = \Delta y = 0.04$ cm. The computational domain had 500 computatonal cells in the x-direction and 80 cells in the y-direction. An average numerical time step, calculated by taking one quarter of the value required by the Courant condition, is approximately 5×10^{-8} s.

Two types of initial states of the primary detonation were used in the two-dimensional simulations. In the overdriven or blast initiation, the initial detonation in the primary explosive is started by depositing excess energy in the form of high temperatures and pressures in a small region of the primary tube that is farthest upstream from the end of the barrier. A detonation quickly develops in the primary mixture, and by the time it has reached the end of the separating barrier (4.0 cm), it is still overdriven. In the CJ initiation, the computed one-dimensional profiles of the density, momentum, energy, pressure, and temperature in the vacinity of the detonation front were used to initialize the planar CJ detonations in the two-dimensional computations.

A number of resolution and other detailed numerical tests were done using these model mixtures and are reported by Jones et al. [1991b]. The essential results are that for the grid size chosen, the profiles of the one-dimensional CJ detonation do not vary with change in Δx. Thus for some purposes, and these will be discussed further in the Discussion section, the detonation computations presented below are adequately resolved.

4. SHOCK STRUCTURES IN EXPERIMENTS AND SIMULATIONS

The special double-layer shock-tube developed for these experiments [Liu et al. 1987, 1988] can use various combinations of energetic and nonreactive gases in the upper and lower layers. This facility consists of two adjacent three-meter long steel detonation tubes containing primary explosive in the top channel and secondary (or bounding) explosive in the bottom channel. The channels terminate in a test section 15 cm long in which the steel barrier between the two explosives has been replaced by a very thin cellulose film. This film prevents the two explosives from mixing before the arrival of the detonation, while providing minimal interference in the shock and detonation transmission process. High-speed Schlieren framing photographs were taken, pressure switches were used to monitor the velocity of the primary detonation, and pressure transducers mounted on the top and bottom walls of the test section provided the pressure history in each channel. The sequence of fifty

Schlieren photographs, each with a 9 ns exposure, show the details of the interaction over a 100 μs period after the beginning of the interaction when the primary detonation first comes into contact with the bounding mixture at the test section. The primary explosive is ignited far upstream by a glow plug.

In the experiments, the detonation tubes contained either stoichiometric or lean mixtures of undiluted hydrogen and oxygen. In the simulations, the detonation tubes contained either stoichiometric or lean mixtures of hydrogen and oxygen, all diluted with argon. The four sets of simulations and experiments described here are:

a. The primary mixture is stoichiometric and the secondary mixture is inert.
b. Both the primary and secondary tubes contain the same and stoichiometric mixture, so that the CJ velocity is the same for both mixtures;
c. The lean mixture is on the top, and the stoichiometric mixture is on the bottom, so that the CJ velocity of the primary explosive is lower than of the secondary.
d. The primary tube contains the stoichiometric, more energetic mixture, and the bottom tube contains the lean mixture.

a. *Primary Mixture Stoichiometric; Secondary Mixture Inert*

Figure 3 shows Schlieren photographs of a detonation propagating in a stoichiometric mixture of hydrogen and oxygen, and then the transmission of this detonation into an inert mixture of hydrogen and nitrogen (H_2:N_2 = 16:1). The first frame is in the bottom left column and the detonation moves from right to left. The interaction in the bounding medium is initiated by an explosive bubble or blast wave (first seen in frame 2) generated by the high pressure behind the primary detonation. This wave expands into the secondary mixture and is then reflected from the lower wall (frame 5). In this case, the transmitted structure becomes an oblique shock and the second half of the photographs (frames 16 and higher) shows a transition from regular to Mach reflection.

Figure 4 shows simulations of an overdriven primary detonation in a dilute stoichiometric mixture transmitted into a mixture of the same composition, but the chemical reactions are not allowed to occur in the inert, bounding material. As in the experiments, an oblique shock is transmitted into the inert bounding mixture after a brief transition period. At first, the reflection at the lower wall is regular, but then the computed reflection pattern becomes more complex than the observed one as the primary detonation becomes highly curved and decelerates. This difference

from the experiments, observed after the initial period, is what would be expected from the leaner mixture used in the simulation. The leaner mixture has a longer induction zone and then, as shown by Dabora et al. [1965], the presence of the inert boundary results in a larger wave curvature and deceleration of the detonation front. The complex structure of the later phases of the reflection at the lower wall is the result of the decelerating primary wave.

b. Stoichiometric Primary and Secondary Mixtures

Figure 5 shows Schlieren photographs of a detonation propagating in a stoichometric mixture of hydrogen and oxygen, and then the transmission into the secondary tube containing the same mixture. Now an oblique shock develops into a Mach reflection in the secondary explosive. In contrast to the case where the secondary bounding material is inert, the Mach stem is replaced by a normal accelerating detonation wave that catches up to the primary wave.

According to shock-polar analysis, a complicating factor when the bounding medium is reactive is that either a detonation or an oblique shock can be transmitted into the bounding medium. Both configurations have been observed in the experiments. Estimates of the induction length behind a transmitted oblique shock indicate that it is so large that it is unikely that an oblique shock initiates a detonation [Liu et al., 1988]. In some cases, it has been found that the initiation of a detonation in the bounding mixture is extremely sensitive to conditions at the interface between the primary and secondary explosive [Liu et al., 1987]. Thus, in Figure 5, even though the bounding medium is reactive, an oblique detonation is not induced directly. Instead, a normal detonation is initiated behind the Mach reflection from the lower wall.

Figure 6 shows the results of a computation in which both the upper and bounding materials are the stoichiometric argon-diluted mixture and the primary detonation is initially overdriven. At first, the initial configuration looks very much like the inerted case described above. However, here a detonation starts behind a Mach reflection at the lower wall and this detonation then catches up to the primary detonation. Because the only difference between the conditions of the simulations shown in Figures 4 and 6 is that the bounding gas is reactive in Figure 6, it appears likely that the accelerating wave is a detonation as in Figure 5, where the striations behind the wave again identify it as a detonation. By step 3000 in the simulation, the final timestep in the calculation, the interaction does not appear to have reached any final, steady configuration. The transverse disturbance (shock wave) formed when the transmitted blast hits the bottom wall is moving upward (after step 1500) and at step 1900, a new disturbance in the front has appeared spontaneously above

it and is also moving up and bounces off the wall at step 2300. By step 2000, the shock formed in the bounding region has gone through a transition to detonation. At step 3000, a single detonation spans the test section. The expected final structure in Figure 6 is a propagating detonation with a highly irregular detonation cell structure, estimated to be approximately 0.1 cm and so significantly smaller than the total height of the tube.

Figure 7 shows pressure contours from a computation for the same mixture, but now the primary detonation is CJ when it reaches the bounding material. These results are qualitatively similar to those obtained for the overdriven primary detonation: a blast wave moves into the secondary detonation tube and initiates chemical reaction in the mixture. The structure of the pressure contours at the front of the detonation wave in the upper tube indicate that the reaction zone has already started to separate from the shock front. By cycle 1200, the blast wave has made an irregular or Mach reflection off the bottom of the lower tube and a strongly coupled reactive shock has formed behind the stem of the reflected shock [Sichel et al., 1990]. After 1400 cycles, the lower wave has just moved ahead of the decaying detonation in the upper channel and thereafter continues to accelerate up to CJ velocity. After 1800 cycles the triple point has reflected off the upper surface of the detonation tube and now a strongly coupled reactive shock spans both channels of the detonation tube and rapidly transitions to a steady CJ detonation. As before, the simulated primary wave is more curved than the experimental results because the simulated mixture is more dilute. However, the main feature of the experiments, that is, the initiation of the secondary detonation behind a Mach reflection at the lower wall, is reproduced by the simulation.

One important experimental diagnostic is the data from the pressure transducers mounted on the top and bottom surfaces of the test section. Figure 8 shows numerical and experimental simulations of the pressure as a function of time at the positions of these transducers. Agreement with the experimental records is excellent. The pressure on the top surface of the test section (Figure 8a) shows the passage of the initial detonation wave, followed by the interaction of the reflected shock with the upper surface of the tube at a later stage. The pressure at the lower station (Figure 8b) shows the initial reflection of the oblique shock wave and then a rapid pressure increase due to the transition to an irregular reflection. The shock then travels up through the test section, is reflected off the upper surface, and then its reflection off the bottom surface is visible towards the end of the trace.

c. Lean Primary Mixture; Stoichiometric Secondary Mixture

Since detonations with this configuration in pure H_2-O_2 could not be ignited, experiments were performed with lean methyl ether and oxygen (C_2H_6O/O_2) in the primary tube with an equivalence ration of 0.5, and stoichiometric undiluted hydrogen and oxygen in the secondary tube. Here the detonation velocity of the ether mixture is less than that of pure, stoichiometric H_2-O_2, but the pressure at the detonation front is greater. The Schlieren photographs for this experiment, shown in Figure 9, show that a detonation initiated in the lower tube soon overtakes the detonation in the upper tube and runs ahead of it.

Results of a sequence of calculated pressure contours is shown in Figure 10 for the dilute, lean hydrogen-oxygen mixture starting at the CJ velocity, and in this case we see that both shocks are decaying and after the initial interaction, no detonation results. After 1000 timesteps, the blast wave has just reflected off the bottom of the lower tube and a Mach stem has formed. However, no reaction has been initiated behind the reflected shock. The contours for the mixture in the upper tube again show decoupling of the reaction front and the shock front and the formation of a wide induction zone. After 3000 timesteps, the simulation shows that the peak shock pressures have decayed and there are wide induction zones for both mixtures. By step 3000, the velocity of the front structure has decayed to 700 m/s and is continuing to decrease with no indication of detonation reignition.

d. Stoichiometric Primary Mixture; Lean Secondary Mixture

When the bounding mixture is lean, the detonation velocity of the primary explosive is greater than that of the secondary explosive, so that any detonation induced in the secondary explosive will be overdriven. Schlieren photographs, Figure 11, show that a complex pattern forms consisting of an oblique detonation near the lower wall and an oblique shock wave nearer to the primary wave. Then an oblique detonation, generated near the bottom of the lower shock tube, is connected by an oblique shock to the interface between the two media. According to the shock-polar analysis [Liou, 1986], both modes of interaction observed in this complex refraction are possible. It is interesting to speculate on the mechanism by which the oblique detonation is generated in this case. It is possible that instabilities due to the interface between the primary detonation products and the unreacted gas behind the oblique shock may provide the initiating disturbance.

Figure 12 shows pressure contours from a numerical simulation in which an overdriven detona-

tion, initially propagating in the stoichiometric argon-diluted mixture, comes in contact with the lean argon-diluted mixture. Elapsed times and numerical timesteps are indicated on the figure, in which the detonation moves from left to right (in contrast to the experimental framing picures, in which propagation is from right to left). The variation of the velocity of the leading shock with time is shown in Figure 13. Here the primary detonation is substantially overdriven wh· it reaches the bounding material. However, the structures formed look very much like those observed experimentally and shown in Figure 11. Starting at 17.4 μs, there is a bubble or blast wave that grows and, at about 28.8 μs, it hits the bottom wall and is reflected, giving reflection patterns that look very much like the experiments shown in Figure 11. Between 28.8 μs and 34.9 μs, the interaction has evolved into what appears as an oblique shock transmitted into the secondary explosive. Then a further transition occurs near the lower wall resulting in what appears to be an oblique detonation. By this time the velocity of the primary detonation has reached a steady value of 1600 m/s. The pressure contours beyond 55.8 μs display the same combined oblique shock and oblique detonation pattern observed in Figure 11.

Figure 14 shows pressure contours from a computation for the same mixtures, but now the detonation in the primary tube is a CJ detonation when it reaches the bounding material. In this case, the results are qualitatively quite different in that the transmitted detonation first appears to die out as the leading shock becomes decoupled from the reaction front. However, it then reignites as a result of a series of shock reflections and propagates as a complex, nonsteady dynamic structure. By timestep 200, the detonation reaches a location where there is no longer a barrier separating it from the mixture in the bottom tube. It then transmits a bubble into the lean mixture below as it continues to propagate in the upper stoichiometric mixture. By step 800, the system has evolved so that the detonation on the top is connected to a very oblique leading shock on the bottom, and the transmitted bubble has reflected from the lower wall. Then the entire system continues to weaken, except for the complex shock structure formed when the bubble reflects from the lower wall. This reflected shock structure steepens and, some time after step 2000, becomes very intense and appears to ignite near the Mach stem formed on the bottom. By steps 2400 or 2600, there are two very strong waves, one on top and one on the bottom, and these continue to grow to form what finally appears to be a reestablished propagating detonation.

Figure 15 shows a history of the mean velocity of the overall structure, taken as the velocity of the leading shock wave. After the detonation reaches the barrier, its velocity decreases with time

to a minimum, after which it starts to increase again after the shock and the reaction front in the upper tube are reunited. We refer to the detonation thus formed as a marginal detonation. In the next section, we examine the extinction and reignition of this marginal detonation in considerable detail, as this provides an important example of what has been referred to as an "explosion within an explosion." This process plays a key role in the reignition of marginal detonations and in deflagration-to-detonation transitions.

5. DECAY AND REIGNITION OF THE MARGINAL DETONATION

Several approaches are possible for describing the complex shock and detonation physics occurring in this system. After some efforts, we decided that describing the evolution of the system as a whole tends to be too confusing. Therefore, we have chosen to break the description into a discussion of:

- the initial detonation transmission and expanding bubble,
- the detonation decay and reignition in the upper, primary material,
- the shock and reignition in the secondary material, and then
- the overall interaction process.

5a. Detonation Transmission

As the detonation expands into the lower tube, the expansion and side relief causes the leading shock to decouple from the reaction front while a blast wave or bubble moves down into the lean material. As the primary detonation passes the barrier, the flow turns around under the barrier and a complex vortical structure forms. Some time before step 700, the bubble shock reflects from the bottom wall and then moves upward. This reflected shock further heats and compresses the unreacted material behind it, perhaps even igniting it. Figure 14 also shows a transverse wave structure at the detonation front in the top half of the tube. This structure initially appears at the contact surface between the two materials and it seems to have been generated by the disturbance whose orgin is the interface between the two materials.

5b. Decay of the Primary Detonation

The originally planar detonation wave propagating in the top channel is weakened by the expansion process occurring below it. For some time, this upper wave structure is characterized by a closely coupled leading shock and a reaction front, at least through step 1400. For example, Figure 16 shows enlargements of the pressure and temperature contours from steps 1200 to 2000. Around the reaction front at step 1200, the coupling between the shock and reaction front is still fairly close

so that this upper wave structure might still be called a detonation. The temperature and density (not shown) contours show the contact discontinuity between the products of the primary mixture and the unburned secondary mixture behind the oblique shock wave. However, between steps 1600 and 1800, the shock and reaction front become more and more decoupled to the point that the upper structure can no longer be called a detonation and, as shown in Figure 15, the primary front continues to decelerate.

The complex structure behind the leading shock, apparent in the temperature contours but not seen in the pressure contours, is a flame-like structure we call a reaction wave. This wave is not a detonation, for while the temperature changes across typical flames are large, pressure changes are usually minimal. The location of the steep gradient behind the leading shock indicates the end of the reaction zone of the detonation, that is, the location at which the gas is fully reacted and energy release is essentially complete. As time advances, the temperature contours of the upper wave structure show more and more separation between the leading shock and the reaction wave until the reaction wave becomes decoupled from the leading shock while the combined system of shocks and reaction waves decays in time. The upper transverse wave, already noted above, appears to reflect from the upper wall and may account for the "wrinkled" shape of the reaction wave shown in steps 1600 to 2000.

5c. The Reflected Bubble Shock

Upstream of the leading shock structure, there is a secondary shock that has developed from the reflection of the bubble off the lower wall. This reflected bubble shock is first evident at step 800. As this shock moves upward in the chamber, it accelerates and moves first into unreacted lean gas and then into the fully reacted gas behind the primary detonation. By step 1600, this shock hits the top wall and produces another reflected shock moving downwards and upstream into fully reacted material and away from the propagating fronts. This second reflected shock subsequently sweeps down in the tube behind the bulk of the structure and finally reflects from the bottom wall near step 2400.

5d. Reignition of the Detonation Wave

Now consider Figure 17, which contains a series of traces of selected parts of the shock and reaction wave in the upper tube. This figure contains a composite of information taken from pressure, density, temperature, and reaction-variable contours. Figure 17a is a sequence showing just the

leading shock and the reaction wave. By step 2000, the reaction front and the leading shock are still separating. Figure 17b repeats step 2000, but now includes the upstream shock that resulted from the bubble reflection. In time, this shock steepens and eventually meets the decaying reaction wave at step 2200. By step 2400, the bubble shock and the reaction wave are now a closely coupled complex, looking somewhat like a detonation, and overtaking the leading shock. This sudden merging of the flame and shock wave initiates the process which, by step 2900, leads to reacceleration of the leading shock front.

The reignition that occurs in the upper tube is a key phenomenon that occurs when a shock wave overtakes a reaction wave, flame, or deflagration. After the shock overtakes the reaction wave, the complex that is formed (the two close contours at step 2400 in Figure 17b) accelerates with respect to the leading shock. This new complex reaction wave is moving at approximately 1600 m/s, which is substantially above the 1200 m/s of the leading shock, and supersonic with respect to the material behind the leading shock. The temperature behind the leading shock is 1200 K, and the speed of sound in this material is about 700 m/s, so that this complex behaves like a strong, high-speed detonation moving through this material. The reignition process thus seems to be associated with the strengthening of the bubble shock.

Ignition of a detonation structure in the lower tube occurs some time between steps 2000 and 2200 near the lower reflecting wall. Figure 18 shows a composite and enlargement of pressure and temperature contours for steps 2200 through 2800. The reaction process occurring on the bottom at step 2200 is similar to a mode of ignition observed in previous simulations and described in detail by Jones et al. [1991a] and Sichel et al. [1990]. Here it intensifies the bubble shock which, as noted above, meets the upper reaction wave and becomes a detonation structure in the upper tube, as is evident in step 2400. Step 2600 shows complex combined shock and detonation structures propagating toward each other from the upper and lower reflecting surfaces. The pressure contours show closely coupled detonation structures on both the top and bottom, connected by a curved shock in the center. At this point, the original leading shock still leads the detonations on the top and bottom. By step 2800, the upper detonation has almost overtaken the leading shock, and by step 3000, as shown in Figure 19, it has merged with the leading shock to form one structure. Until this time, the velocity of the combined detonation structure has been constantly decaying to below the CJ value of the upper mixture, but it has never decayed to below the CJ velocity of the lower mixture. Near step 2900, as seen in the velocity-history profile in Figure 15, the velocity of the combined structure suddenly begins to increase.

5e. The Final (?) State

In computations of the type reported here and in experiments, there is always the question whether the detonating system has reached a final steady state mode of propagation. The present calculations have been extended to 5000 time steps. By this time reignition has occurred separately in both the top and bottom mixtures and the resultant detonations have merged to form the configuration shown in Figure 19. The system has evolved into an approximately normal detonation in the primary mixture connnected by an oblique shock to a detonation in the lower, secondary mixture. This configuration is similar to those observed experimentally [Liu et al. 1988] when the primary H_2-O_2 mixture is stoichiometric and the secondary mixture is lean, but here, too, it is not entirely clear whether the interaction has reached a final steady state at the end of the observation period. Figure 15 shows that by the time the computation was terminated at step 5000, the velocity of the complex had not reached its final value, but was still increasing.

6. DISCUSSION

In this paper, we have summarized a series of numerical computations describing the glancing interaction of a detonation in a diluted stoichiometric hydrogen-oxygen mixture with a bounding layer of inert or explosive material. Four sets of simulations are described: a) the primary mixture is stoichiometric and the secondary mixture is inert; b) both the primary and bounding layer contain the same and stoichiometric mixture, so that the CJ velocity is the same for both mixtures; c) the primary mixture is lean and the bounding mixture is stoichiometric, so that the CJ velocity of the primary explosive is lower than that of the secondary; and d) the primary tube contains the stoichiometric, more energetic mixture, and the bottom tube contains the lean mixture.

While the simulations considered dilute hydrogen-oxygen mixtures, experimental data was available from previous experiments conducted using undiluted mixtures as well as methyl ether with pure hydrogen-oxygen. However, the relative values of the CJ velocities of the primary and bounding mixtures are the main parameters governing the interaction and these were reproduced in the simulations. By comparing the computed complex shock-detonation structures to those obtained in similar experiments, we were able to gain confidence in the predictions of the simulations as well as note important similarities and differences. We observed that the simulations generally reproduced the overall interacion patterns observed in the experiments. This is particularly true

for comparisons between the computations of overdriven primary detonations in diluted hydrogen-oxygen mixtures to CJ detonations in the undiluted mixtures. This agreement in the resulting structure occurs because the extra energy associated with the overdriven primary detonation compensates for the effects of dilution.

In every case, the primary detonation expands into the bounding material as a blast wave that eventually hits a containing wall. Then depending on the degree of overdrive and the properties of the two explosives,

- the detonation may die out as it expands into the bounding medium as the accompanying side relief causes the primary shock front to decouple from the reation wave,
- the bounding mixture is energetic enough or the transmitted bubble shock is strong enough so that the transmitted detonation reignites before the transmitted bubble shock reflects,
- the reflection of the bubble shock causes ignition behind it in the twice-shocked, unreacted material,
- the reflected bubble shock itself is not hot enough to cause immediate ignition in the reflected shock region, but because of the curved bubble shock reflecting from the bounding wall, a double Mach reflection results and the resultant high temperatures and pressures cause ignition.

All of these scenarios are observed in the simulations and in the experiments.

Once the system reignites, it can evolve into one of a number of complex configurations consisting of shocks and oblique and curved detonations. As already indicated, a key element determining the interaction between the explosive layers appears to be the relation between the CJ velocities of the two mixtures, which determines whether or not the detonation in the secondary explosive is overdriven by the primary explosive. The situations described here are sufficiently dynamic and complex, so that they cannot be described by classical steady-state theories based on shock and detonation polars, although the results of such analysis do provide some guide to the final configuration [Liou 1986]. Thus when the secondary wave is sufficiently overdriven by the primary wave, the polar theory predicts that the transmitted wave will be either an oblique shock or, if conditions are favorable to initiation, an oblique detonation. As already indicated, this simple theory provides no indication as to which of these final configuration will arise; this depends on unsteady processes of the type treated here.

For the overdriven computations that compare most closely with the undiluted hydrogen-oxygen experiments,

- When the bounding material is inert, regular or Mach reflection occurs at the lower boundary and the complexity of the resulting combined structure seems to depend on the mixture. In the simulations, the propagating detonation becomes highly curved, and a very complex shock structure forms that moves steadily through the system. The undiluted mixtures used in the experiments also show a transition from regular to Mach reflection, but a relatively simpler structure results.
- When the bounding material is identical to the primary explosive, complicated transient structures develop initially. Then if the primary detonation is strong enough to impart sufficient impulse to the unreacted material, the final structure would be a single propagating detonation with a cellular pattern characteristic of the material. The initial stages of this transition appear to be what is observed in both the experiments and the simulations. When the primary detonation is relatively weak, the whole detonation system could decay.
- In some cases of a lean bounding explosive, the experiments show a complex pattern consisting of an oblique detonation near the lower wall and an oblique shock wave. The simulations show structures that look very much like those seen in the experiments, again showing the propagating detonation connected to an oblique shock which, in turn, is connected to an oblique detonation. However, at the time the simulation was terminated, it did not appear that the configuration had reached a steady-state pattern.

Comparisons of simulations with CJ and overdriven primary detonations show that the mode of initiation can significantly affect the development of the interaction, a result that is in accord with many experimental observations. In particular, we consider the simulation of the stoichiometric mixture into the lean mixture. For the overdriven case, specifically a case where the velocity of the primary detonation was 54% over CJ, the system quickly evolves into a structure that propagates at the CJ velocity of the primary mixture. For the case where the primary detonation starts at CJ velocity, the detonation almost dies out, but then reignites due to subsequent ignition in a Mach stem that forms as the curved bubble shock reflects.

The sudden explosive reignition occurring in the Mach stem of the reflected bubble shock is similar to the mechanism reported in experiments by Teodorczyk et al. [1989]. These authors studied the propagation of quasi-detonations, which are detonations that propagate in very rough tubes at speeds substantially below the CJ velocity. In a series of experiments showing the propagation of a detonation over an obstacle and the diffraction of a detonation from a corner, they noted the

importance of shock reflections from the wall in the overall reinitiation process. If they delayed the reflections by changing the spacing of obstacles or walls, the transition to the quasi-detonation state is delayed. These experiments also showed that if the Mach stem formed on shock reflection is strong enough, the detonation can reignite.

Sichel [1990] compared the framing Schlieren photographs of the diffraction at a step of a stoichiometric H_2–O_2 detonation at a pressure of 120 torr [Teodorczyk et al. 1989] and the results of the simulation of a layered detonation where both the primary and secondary mixtures were the same dilute stoichiometric H_2–O_2 mixture described above [Jones et al. 1991a]. A comparison of Fig. 6 from Teodorczyk with Fig. 10 from Jones showed that the main features of the diffraction were reproduced by the simulation. The two configurations are somewhat different: one case is diffraction at a step and the other is an interaction between two layers. The two explosive mixtures being compared also are different, but the low pressure in the experiments tends to increase induction and reaction distances in the same way as the argon dilution of the mixture considered in the simulation. In this sense the simulation mirrors the experiment, as is supported by the fact that the simulation reproduces the main features of the observed interaction.

The exact physical mechanism by which this reignition of the decaying detonation occurs is not clear and two different mechanisms are possible here: the detonation can reignite by autoignition as a consequence of adiabatic shock heating or vortex mixing in the shear layer near the wall behind the Mach stem. It is clear from many computations that the wave structure behind the Mach stem is complex and there are regions where shocks intersect and the temperature reaches the ignition temperature. There are also shear layers entraining and mixing material that has chemically reacted in varying amounts. In the present simulations, we have not been able to say definitively which of these mechanisms is responsible for the observed ignition because there is insufficient resolution in the computations. However, the nature of this ignition process is now being examined in some detail both by theory and computations. The ignition near the Mach stem coincides with an acceleration and straightening of the bubble shock so that it interacts with the reaction front in the upper wave structure. The interaction of the bubble shock and reaction front accelerates the reaction front so that a detonation is formed in the top layer and this detonation moves and eventually combines with the leading shock to form one structure.

There are several points on which it is interesting to speculate. First, if the tube were wider, would the detonation reignite? Another way of asking this question is to ask, how important is the

bounding bottom wall in the reignition process? The process described above could not happen without the presence of the reflected bubble shock, which results in both the lower Mach stem and the upper shock-flame interaction. Even when there are no obstacles to cause reflection when a material is heated long enough, ignition occurs "spontaneously." Thus ignition might seem to occur spontaneously or perhaps the detonation might never die if either the bounding medium is more energetic or if the primary detonation is overdriven. This effect provides an alternate reignition mechanism to what we see in the situation simulated above.

The medium behind the detonation is subject to an extremely complex combination of shocks, reaction zones, and slip lines. The phenomena observed in the present simulation can be considered examples of "explosions within explosions," a phrase first used by Urtiew and Oppenheim [Urtiew and Oppenheim 1965, 1966; Oppenheim et al. 1975], and recently summarized and extended in concept by Sichel [1990]. The idea expressed by this phrase is rather general: an explosive mixture is sensitized through a sequence of gas-dynamic, physical, or chemical processes to the point where a small disturbance is enough to set off rapid exothermic chemical reaction processes leading to detonation.

Consider a planar detonation propagating at the CJ velocity in a medium bounded by perfectly reflecting walls. This configuration is inherently unstable. If the computational resolution were high enough and the system were perturbed, we would see the planar front change to one with dynamically changing shock structure [Oran et al. 1981, Kailasanath et al. 1985, Oran et al. 1988]. In fact, a real detonation in this mixture has a complex structure at the front consisting of interacting incident shocks, Mach stems, and transverse waves that produce the complex pattern of triple points that, when regular enough, lead to what are called detonation cells. However, because the numerical algorithm is conservative, with the choice of model parameters the detonation propagates at the correct velocity, and structures on scales large compared to the cell size can be expected to be fairly accurate. This is substantiated by the similarity noted by Jones et al. [1991a] among computational and laboratory experimental results, and we generally expect this to be true as long as the detonation cells are small enough compared to the larger-scale flow structures of interest here. We therefore assume that the multidimensional calculation on the scale of the phenomena observed is converged enough so that further refining the computational grid would only show more small-scale structure, but would not change the basic properties of the large-scale structure we see. This last observation has been verified to some extent in a series of extremely

resolved computations by Kailasanath et al. [1990] and by the agreement between the simulated and observed detonation diffraction patterns at a step. In order to begin to resolve the complex cellular shock structure at the shock front, we would require a computation with about 1000 computational cells in the vertical direction, and perhaps about 2000 in the horizontal direction. Such compressible computations with simplified chemistry models, while now certainly possible, would require the largest supercomputers. The advantages to be gained from such extensive calculations are not clear at this point, especially since at the relatively high pressure of 1 atm of this simulation, we expect the microscopic structure to be very irregular causing the detonation to appear almost planar on our more macroscopic scale.

In light of the discussion above, some comments on the relative dimensions of the observed detonation cell size λ and the width of the detonation channels are appropriate. Extrapolations from data in Strehlow [1984] indicate an approximate cell size of 0.1 cm for the stoichiometric mixture at standard temperature and pressure. The dilute mixture will have an even larger detonation cell size, estimated to be about 0.5 cm. The lateral dimension of each of the detonation tubes is 1.6 cm, so that there would be approximately 16 detonation cells across the top tube but the secondary mixture might only support about three cells. The 13λ criterion states that a detonation will not propagate from a cylindrical tube of diameter d into a larger space unless $d > 13\lambda$. This criterion, however, depends very much on the geometry. The present simulations are two-dimensional and so correspond to a detonation propagating through a rectangular channel with an effectively infinite aspect ratio, and under these conditions the recent survey by Guirao et al. [1989] indicates that the detonation will be reestablished if the channel width is greater than 3λ. A further constraint is that detonations can propagate in circular tubes only if the criterion $\pi d > \lambda$ is satisfied. For the conditions considered here, the number of detonation cells within the system is large enough to meet these criteria. In this context, it should also be noted that the 13λ or 3λ criteria are based on discharge into an infinite medium. Both the experiments and simulations described here suggest these criteria may no longer be applicable when obstacles or confining walls are present.

A typical computation required approximately 25 μs/timestep/computational cell on a Cray X-MP/14. As with many large-scale multidimensional calculations, we have reached the point where the computational time is considerably less than the analysis time of the output and time taken to generate the diagnostics. This is certainly true for complex two-dimensional calculations and would be even more true for three-dimensional calculations, where the graphical display capabilities are even more rudimentary.

Acknowledgments

The computations were performed on a Cray X-MP/14 with funding provided by the Materials Research Laboratory. This work was sponsored in part by the Naval Research Laboratory through the Office of Naval Research and in part by U.S. Army Research Office under grant No. DAAL03-87-K-0019.

References

Bartlmä, F., and Schröder, K., 1986, The Diffraction of a Plane Detonation Wave at a Convex Corner, *Combustion and Flame* 66, 237–248.

Boris, J.P., and Book, D.L., 1976, Solution of the Continuity Equation by the Method of Flux-Corrected Transport, *Methods in Computational Physics*, Vol. 16, pp. 85–129.

Burks, T.L. and Oran, E.S., 1981, *A Computational Study of the Chemical Kinetics of Hydrogen Combustion*, NRL Memorandum Report 4446, Naval Research Laboratory.

Dabora, E.K., Nicholls, J.A., and Morrison, R.B., 1965, The Influence of a Compressible Boundary on the Propagation of Gaseous Detonations, *Proceedings of the Tenth Symposium (International) on Combustion*, p. 817.

Dabora, E.K., Desbordes, D., Guerraud, C., and Wagner, H.Gg., 1991, *Dynamics of Detonations and Explosions: Detonations*, ed. A.L. Kuhl, J.-C. Leyer, A.A. Borisov, and W.A. Sirignano, *Progress in Aeronautics and Astronautics*, Vol. 133, 187–201.

Fan, B.C., Sichel, M., and Kauffman, C.W., 1988, Analysis of Oblique Shock-Detonation Wave Interactions in the Supersonic Flow of a Combustible Medium, AIAA Paper AIAA-88-0441.

Fickett, W., and Davis, C.W., 1979, *Detonation*, University of California Press, Berkeley.

Gubin, S.A., and Sichel, M., 1977, Calculation of the Detonation Velocity of a Mixture of Liquid Fuel droplets and a Gaseous Oxidizer, *Comb. Sci. Tech.*, 17, 109-117.

Guirguis, R., Oran, E.S., and Kailasanath, K., 1986, Numerical Simulations of the Cellular Structure of Detonations in Liquid Nitromethane — Regularity of the Cell Structure, *Combustion and Flame*, Vol. 65, pp. 339–366.

Guirguis, R., Oran, E.S., and Kailasanath, K., 1987, The Effect of Energy Release on the Regularity of Detonation Cells in Liquid Nitromethane, *Proceedings of the 21st Symposium (International) on Combustion*, The Combustion Institute, Pittsburgh, pp. 1659–1668,

Guirao, C.M., Knystautas, R., and Lee, J.H., 1989, *A Summary of Hydrogen-Air Detonation Experiments*, Rept. NUREG/CR-4961, Nuclear Regulatory Commission, Washington, DC.

Hertzberg, A., Bruckner, A.P., Bogdonoff, D.W., 1988, Ram Accelerator: A New Chemical Method for Accelerating Particles to Ultrahigh Velocities, *AIAA J.* 26, 195–203.

Jones, D.A., Sichel, M., Guirguis, R., and Oran, E.S., 1991a, *Dynamics of Detonations and Explosions: Detonations*, ed. A.L. Kuhl, J.-C. Leyer, A.A. Borisov, and W.A. Sirignano, *Progress in Aeronautics and Astronautics*, Vol. 133, 202–220.

1990a, *Numerical Simulation of Layered Detonations*, to appear in *Progress in Aeronautics and Astronautics*, AIAA, Washington.

Jones, D.A., Oran, E.S., Guirguis, R., 1991b, *A One-Dimensional Flux-Corrected Transport Code for Detonation Calculations*, to appear as an MRL Research Report, Materials Research Laboratory, Victoria, Australia, and also as an NRL Memorandum Report, Naval Research Laboratory, Washington, DC.

Kailasanath, K., Oran, E.S., and Boris, J.P., 1985, Determination of Detonation Cell Size and the Role of Transverse Waves in Two-Dimensional Detonations, *Combustion and Flame*, Vol. 61, pp. 199–209.

Kailasanath, K., Ganguly, K., and Oran, E.S., 1990, Detailed Structure of Two-Dimensional Detonations, K. Kailasanath and E.S. Oran, in preparation for submission to *Combustion and Flame*.

Kaplan, C., and Oran, E.S., 1990, A Numerical Study of Spontaneous Propane Ignition in a Partially Confined Volume, submitted to the *Third International Symposium on Fire Safety Science*, Edinburgh, Scotland.

Korobeinikov, V.P. , Levin, V.A., Markov, V.V., and Chernyi, G.G., 1972, *Astronautica Acta* , 17, 529.

Liou, J.J., 1986, Analysis of the Wave Interaction Between a Propagating Detonation and a Bounding Explosive Layer, Ph.D. Thesis, Department of Aerospace Engineering, The University of Michigan, Ann Arbor, Michigan, MI.

Liu, J.C., Liou, J.J., Sichel, M., Kauffman,C.W., and Nicholls, 1987, J.A., Diffraction and Transmission of a Detonation into a Bounding Explosive Layer, *Proceedings of the 21st Symposium (International) on Combustion*, The Combustion Institute, Pittsburgh, pp. 1659–1668.

Liu, J.C., Sichel, M., and Kauffman, C.W., 1988, The Lateral Interaction of Detonating and Detonable Gaseous Mixtures, *Progress in Astronautics and Aeronautics*, Vol. 114, pp. 264-283.

Matsui, H., and Lee, J.H., 1979, On the Measure of the Relative Detonation Hazards of Gaseous Fuel-Oxygen and Air Mixtures, *Proceedings of the 17th Symposium (International) on Combustion*, The Combustion Institute, Pittsburgh, pp. 1269–1280.

Oran, E.S., and Boris, J.P., 1987, *Numerical Simulation of Reactive Flow*, Chap. 8, Elsevier, New York.

Oran, E., Boris, J.P., Young, T.R., and Picone, J.M., 1981, Numerical Simulations of Detonations in

Hydrogen-Air and Methane-Air Mixtures, *Proceedings of the 18th Symposium (International) on Combustion*, The Combustion Institute, Pittsburgh, PA, pp. 1641–1649.

Oran, E.S., Kailasanath, K., and Guirguis, R.H., 1988, Numerical Simulations of the Development and Structure of Detonations, *Progress in Astronautics and Aeronautics*, 114, 155–169.

Oppenheim, A.K, Cohen, L.M., Cheng, R.K., Hom, K., 1975, *15th Symposium (International) on Combustion*, p. 1503, The Combustion Institute, Pittsburgh.

Sheng, Y., and Sislian, J.P., 1985, A Model of a Hypersonic Two-Dimensional Oblique Detonation Ram Jet, University of Toronto Institute of Aerospace Studies, Tech. Note 257.

Sichel, M., 1990, Transition to Detonation – Role of Explosion within an Explosion, *Proceedings of the NASA Combustion Workshop*, to be published by Springer, New York.

Sichel, M., Jones, D.A., Oran, E.S., and Guirguis, R., 1990, *Detonation Transmission in Layered Explosives*, to appear, *Proceedings of the 23rd Symposium (International) on Combustion.*

Strehlow, R.A., 1984, *Combustion Fundamentals*, p. 307, McGraw Hill, New York.

Taki, S. and Fujiwara, T., 1981, Numerical Simulation of Triple Shock Behavior of Gaseous Detonation, *Eighteenth Symposium (International) on Combustion*, pp. 1671–1681, The Combustion Institute, Pittsburgh, PA.

Teodorczyk, A., Lee, J.H.S., and Knystautas, R., 1989, *Twenty-Second Symposium (International) on Combustion*, p. 1723–1731, The Combustion Institute, Pittsburgh, PA.

Urtiew, P.A., and Oppenheim, A.K., 1965, *Combust. Flame*, 9, 405.

Urtiew, P.A., and Oppenheim, A.K., 1966, *Proc. Roy. Soc.*, A295, 13–28.

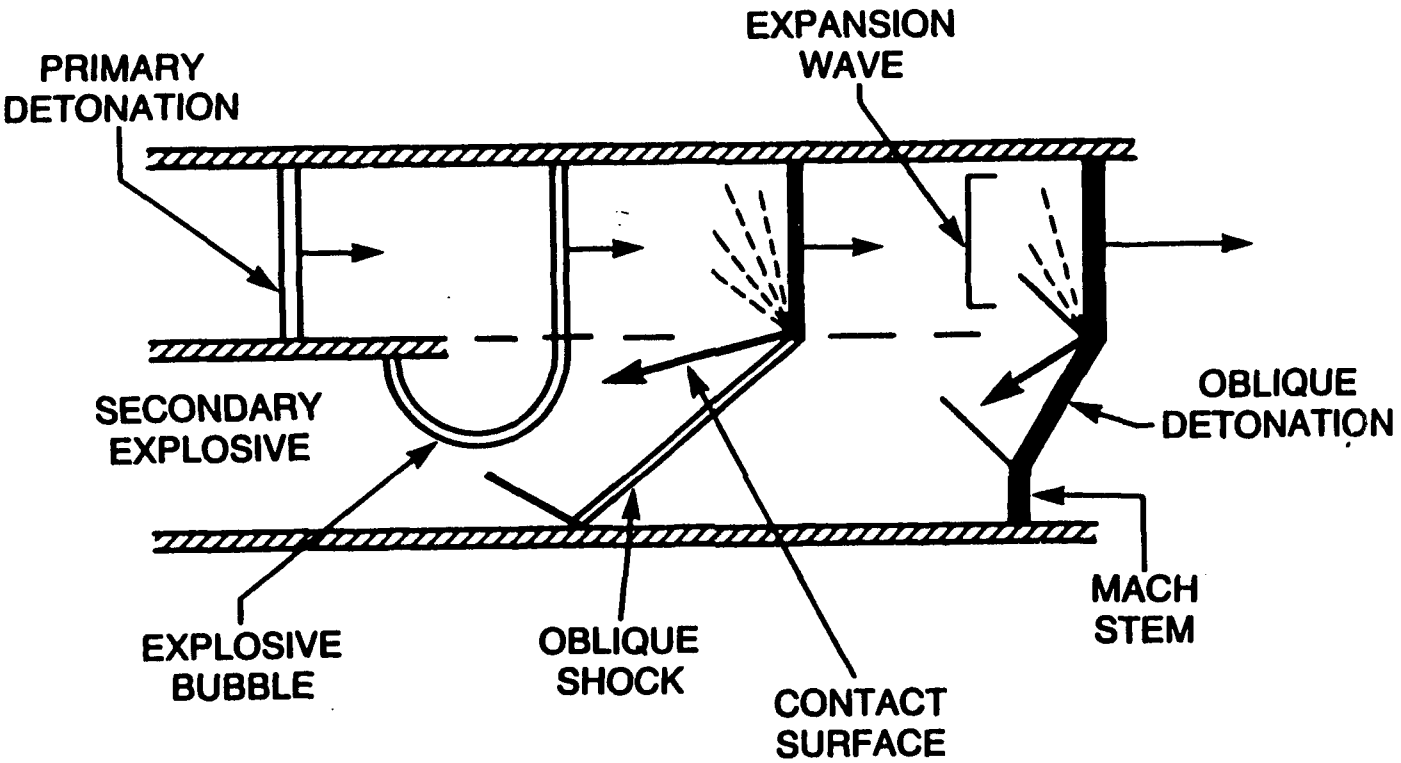

Figure 1. Typical patterns for the layered detonation interaction.

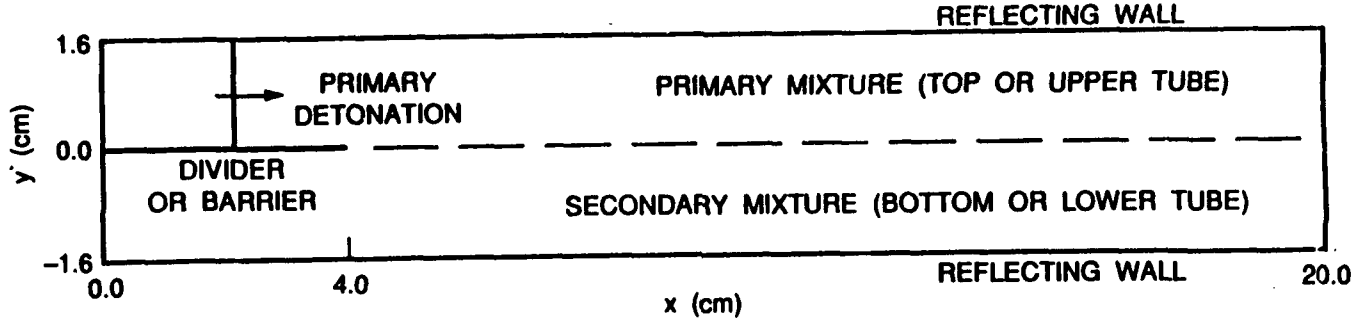

Figure 2. Schematic of the computation domain.

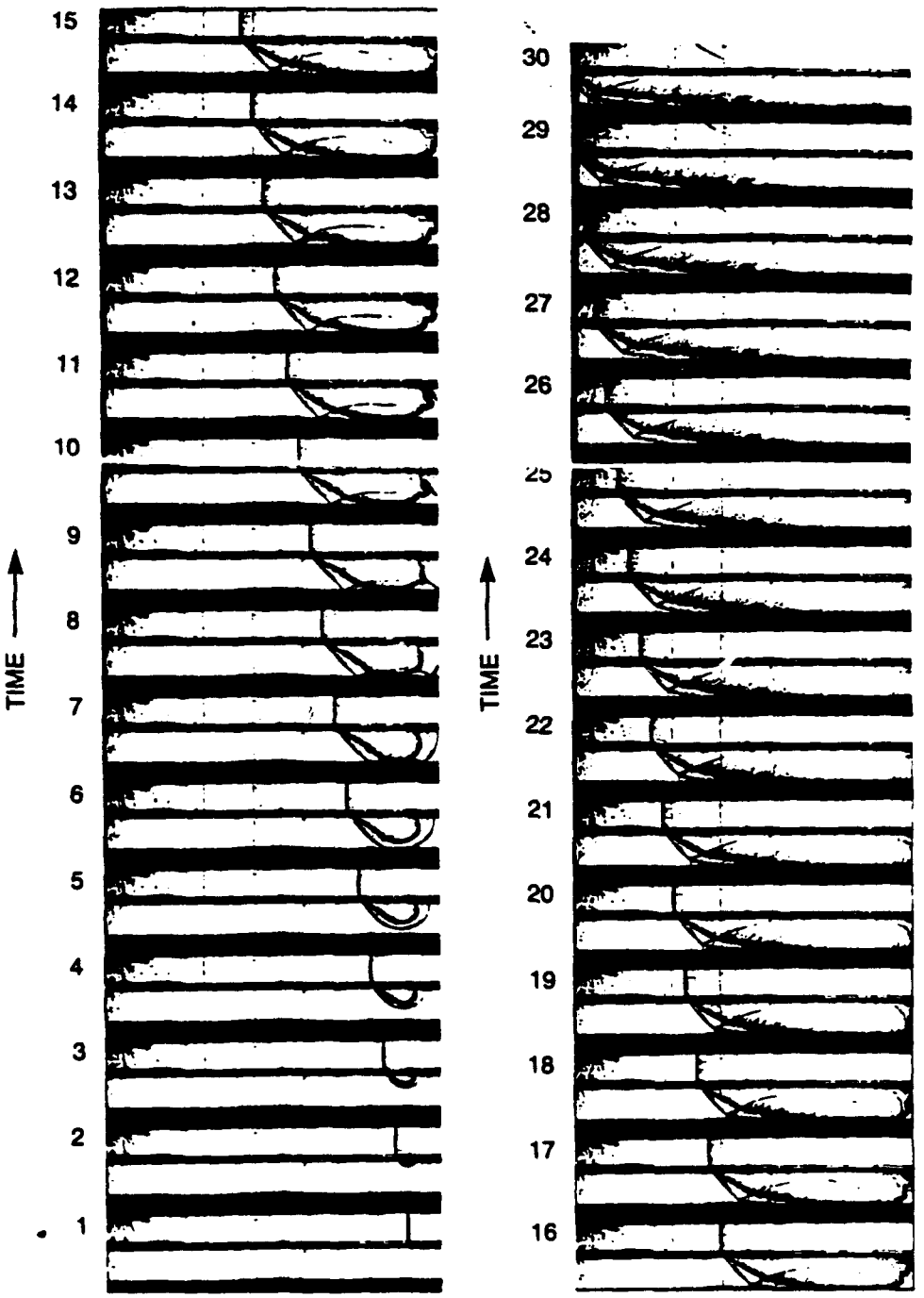

Figure 3. Schlieren framing photographs, inert secondary mixture. Primary mixture H_2:O_2/2:1; secondary mixture (inert) H_2:N_2/16:1. Note that the detonation is moving from right to left.

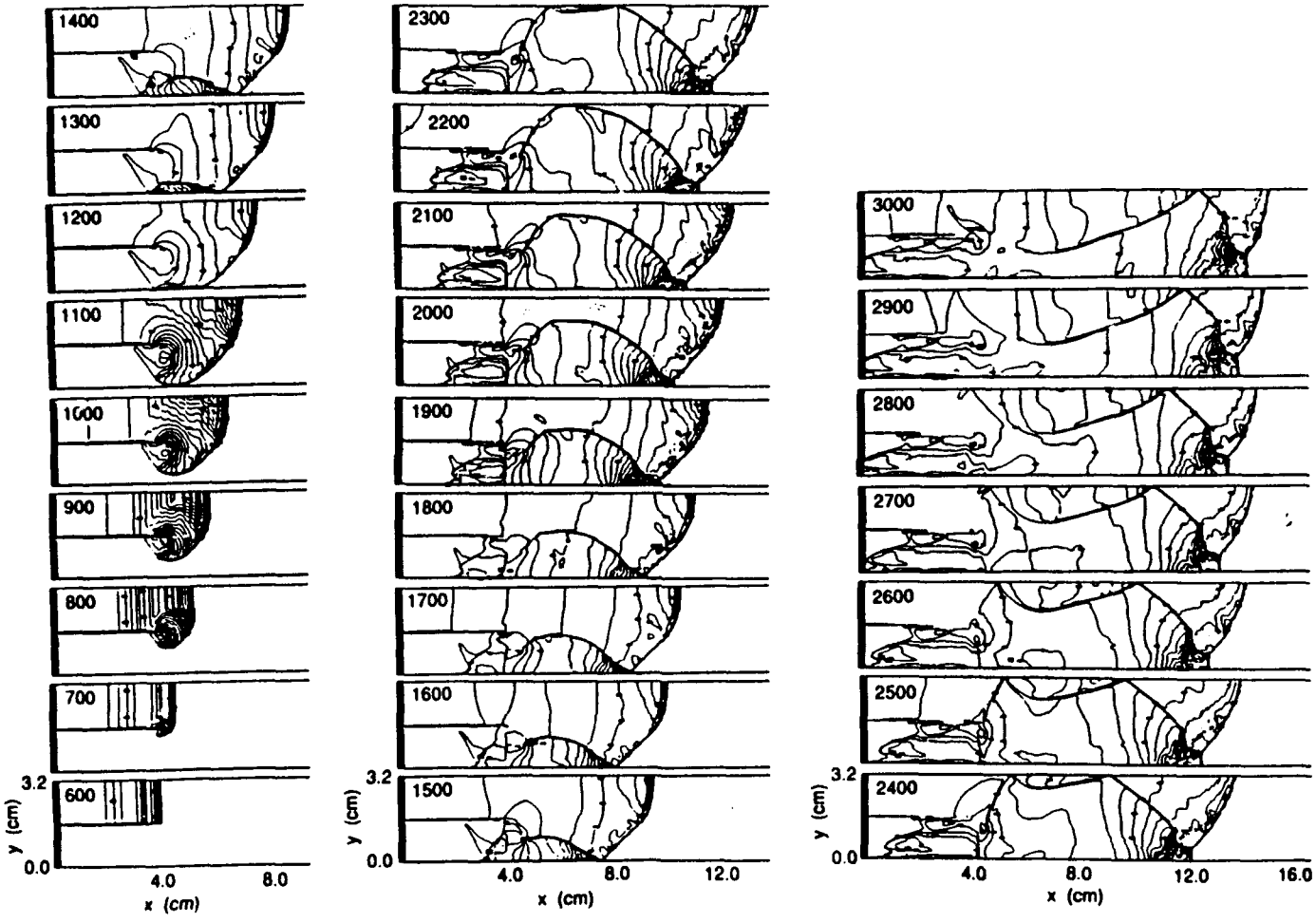

Figure 4. Constant pressure contours from numerical simulation. Primary (upper) mixture H_2:O_2:Ar/2:1:7; secondary (lower) mixture H_2:O_2:Ar/2:1:7 (inerted).

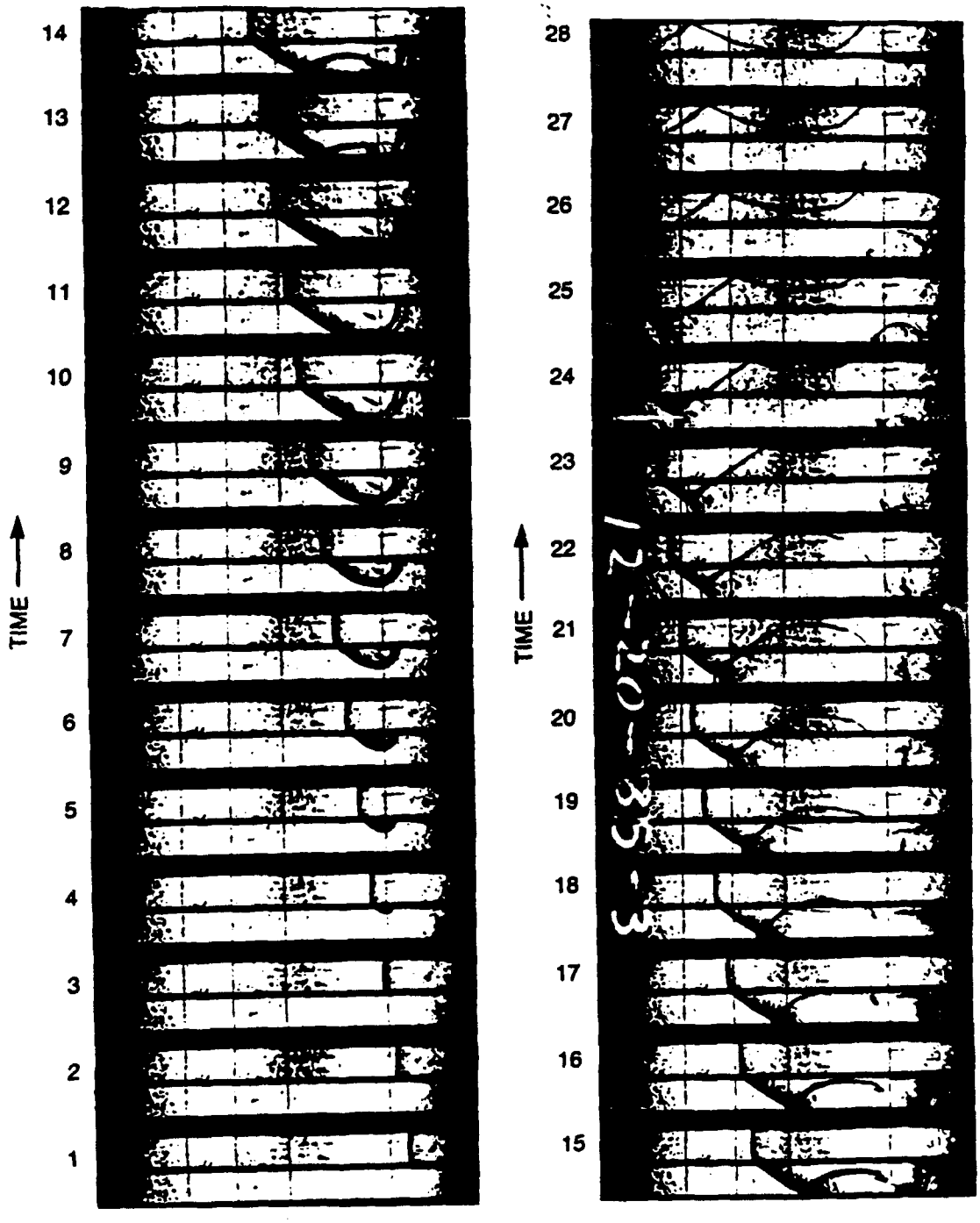

Figure 5. Schlieren framing photographs (same mixtures as Figure 4, but now the secondary mixture is allowed to react). Primary Mixture H_2:O_2/2:1; secondary mixture H_2:O_2/2:1.

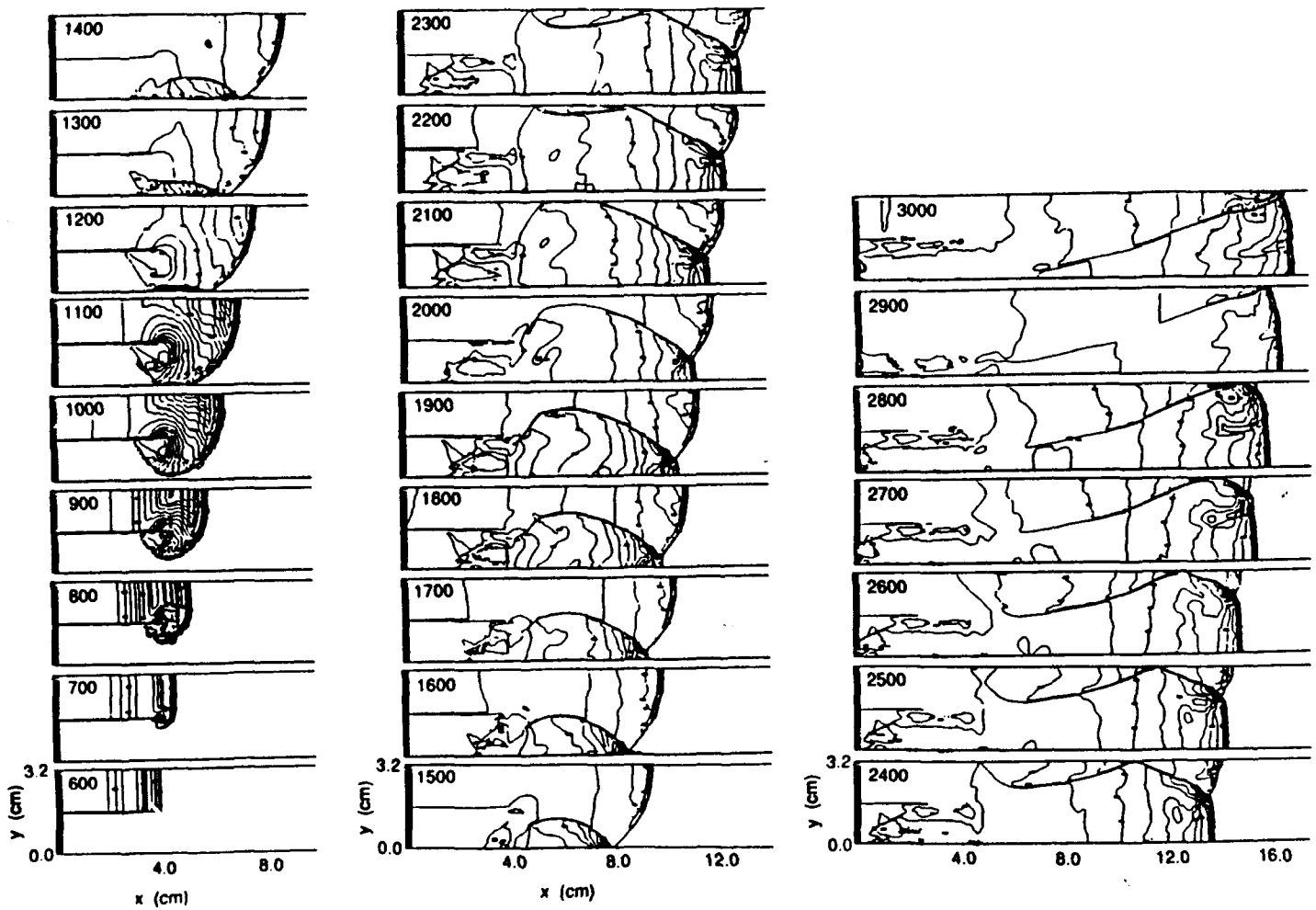

Figure 6. Contours of constant pressure from numerical simulation. Primary (upper) mixture H_2:O_2:Ar/2:1:7; secondary (lower) mixture H_2:O_2:Ar/2:1:7. Primary detonation is initially overdriven.

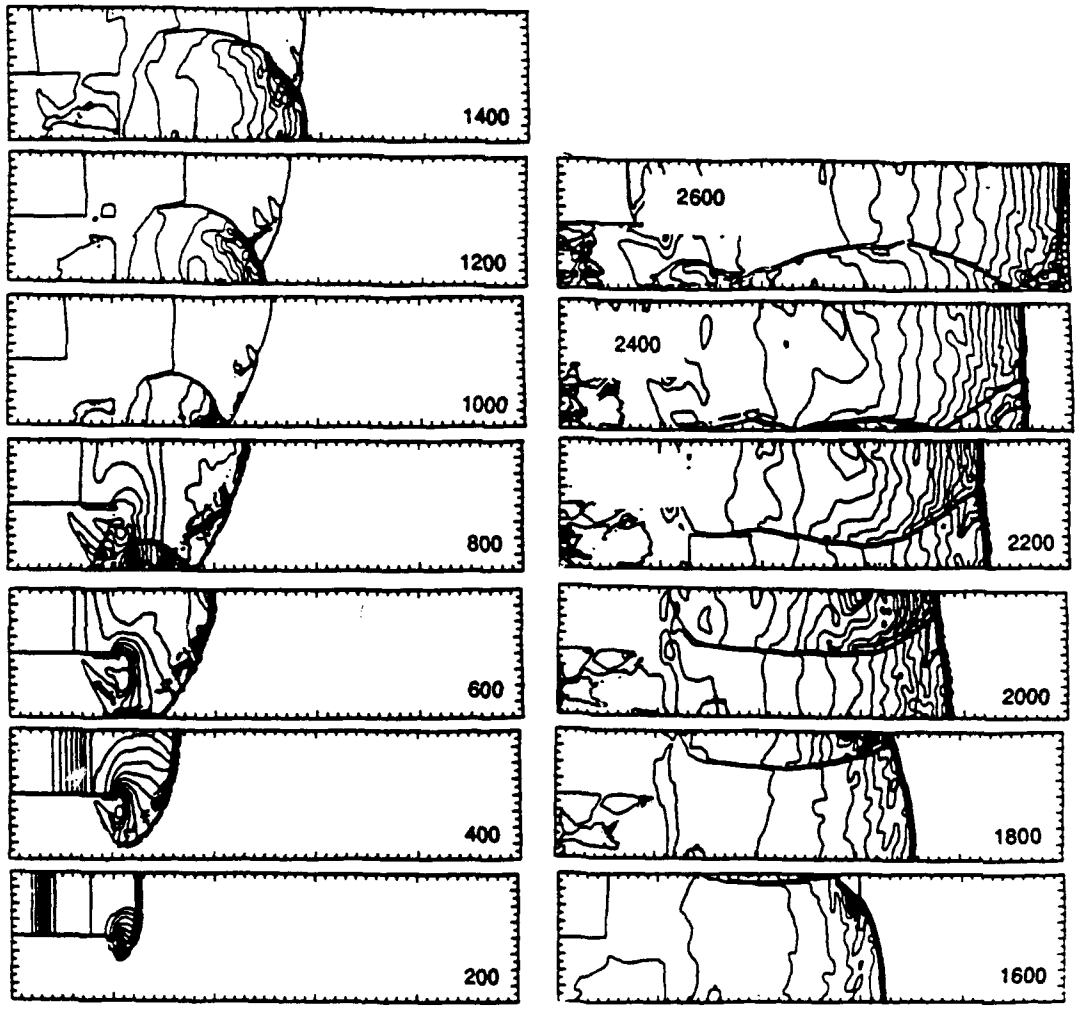

Figure 7. Same mixtures as Figure 6, but primary detonation is initially CJ.

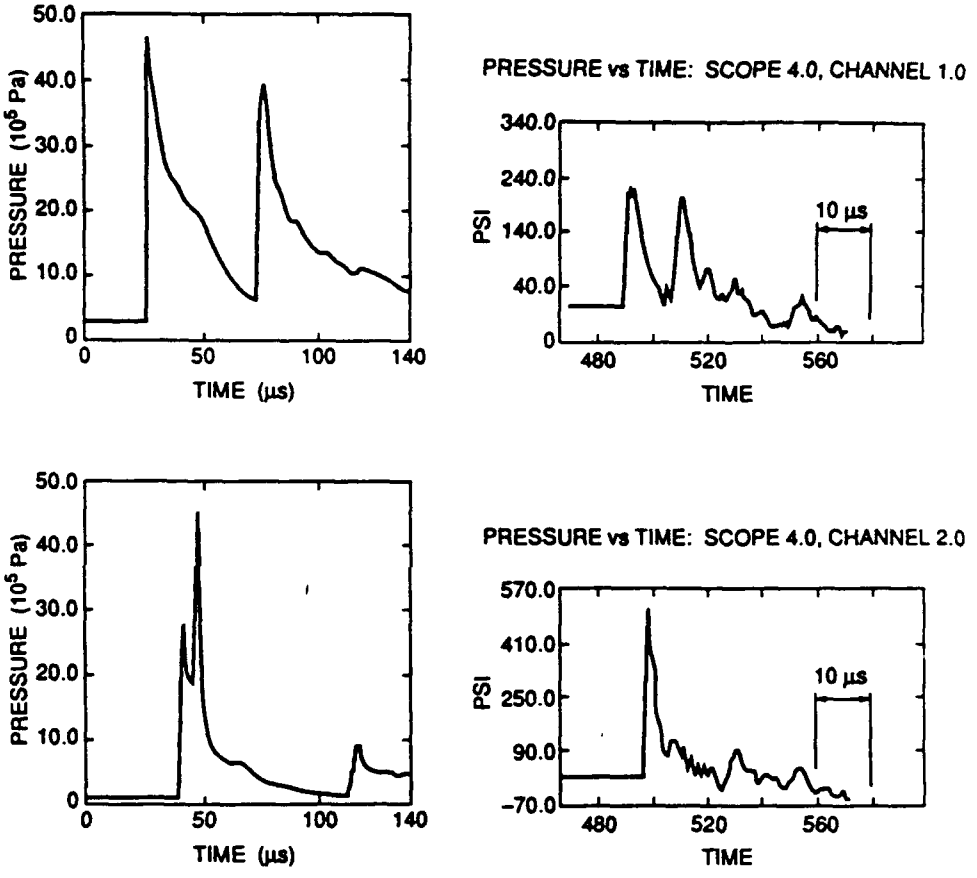

(a) Simulated pressure contours (b) Measured pressure contours

Figure 8. Simulated and experimental pressure traces at the top and bottom of the test section for the case of a stoichiometric mixture in both primary and secondary tubes and a CJ detonation in the primary mixture.

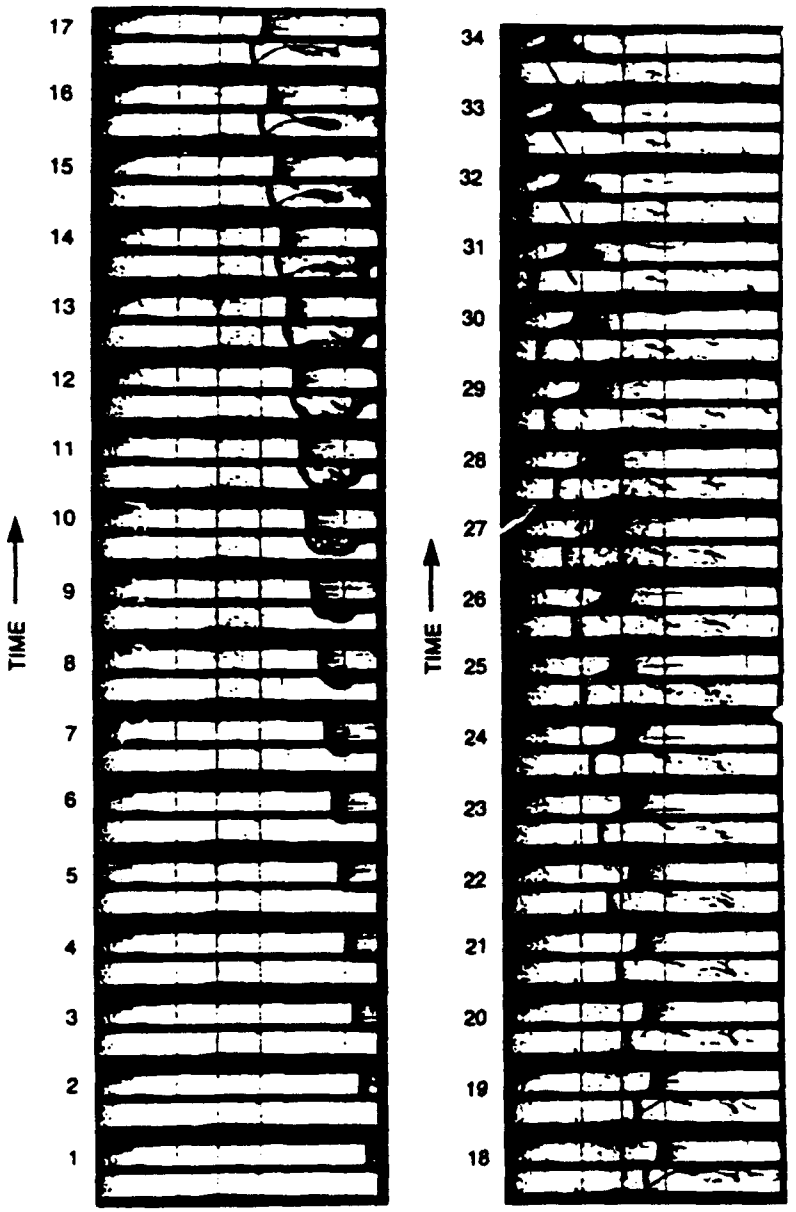

Figure 9. Schlieren photographs for detonation generated with methyl ether (C_2H_6O/O_2), equivalence ratio of 0.5, in the primary tube and stoichiometric undiluted hydrogen and oxygen in the secondary tube.

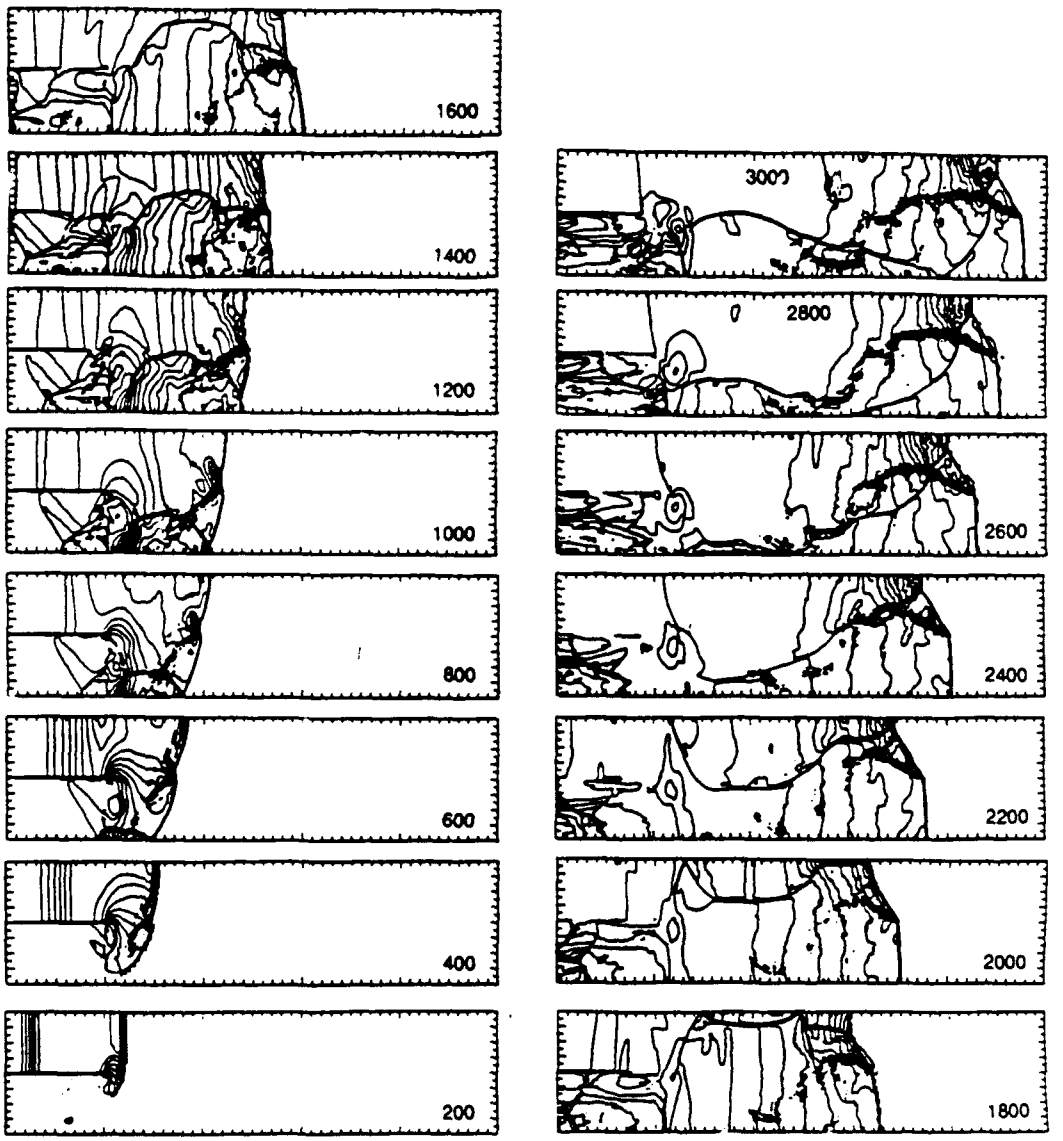

Figure 10. Simulated pressure contours for a primary detonation propagating at CJ velocity in a dilute, lean hydrogen-oxygen mixture, propagating into a stoichiometric secondary mixture.

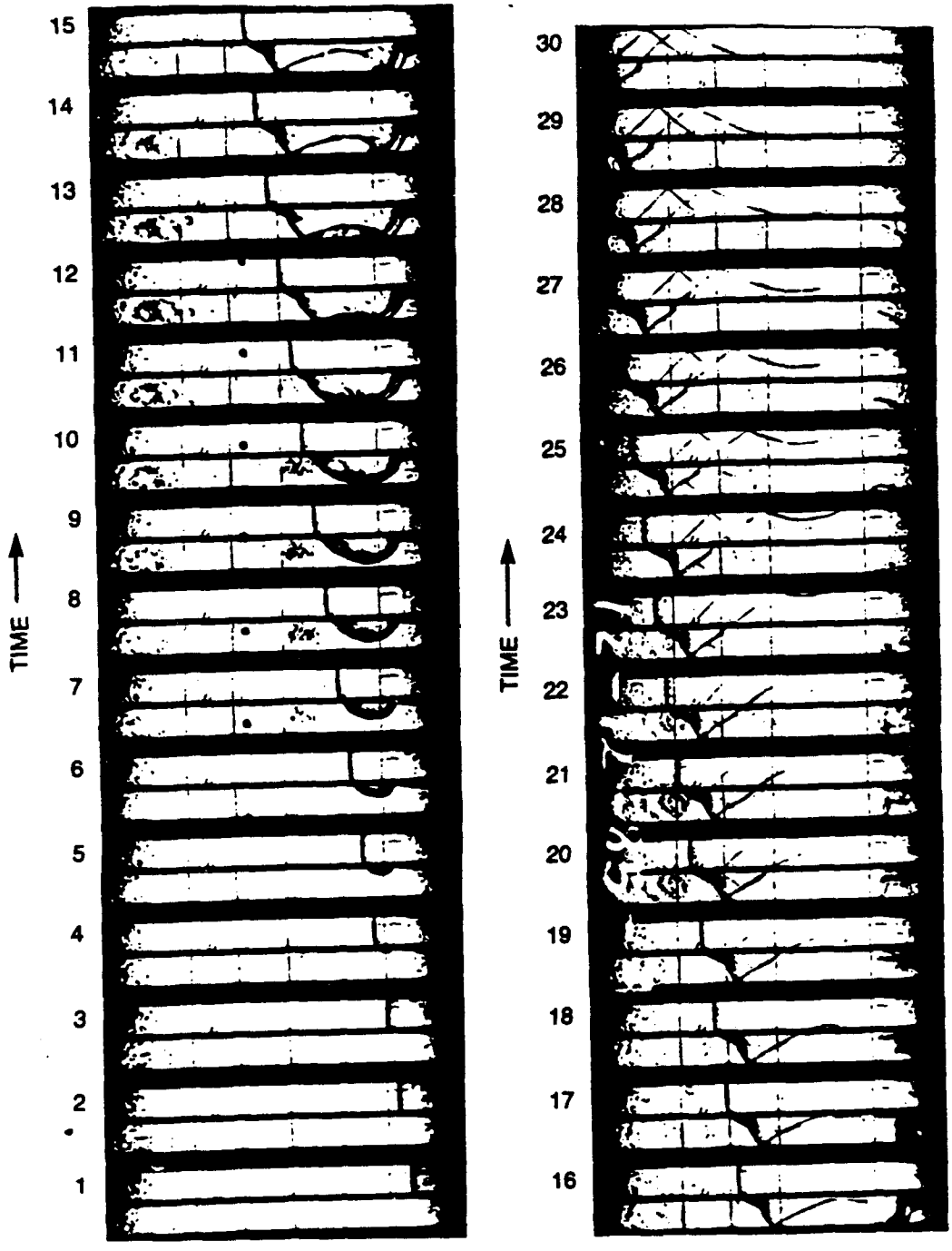

Figure 11. Schlieren photographs for detonation initiated in a stoichiometric primary mixture and a lean bounding mixture. Primary mixture H_2:O_2/2:1; secondary mixture H_2:O_2/0.9:1, ϕ = 0.45.

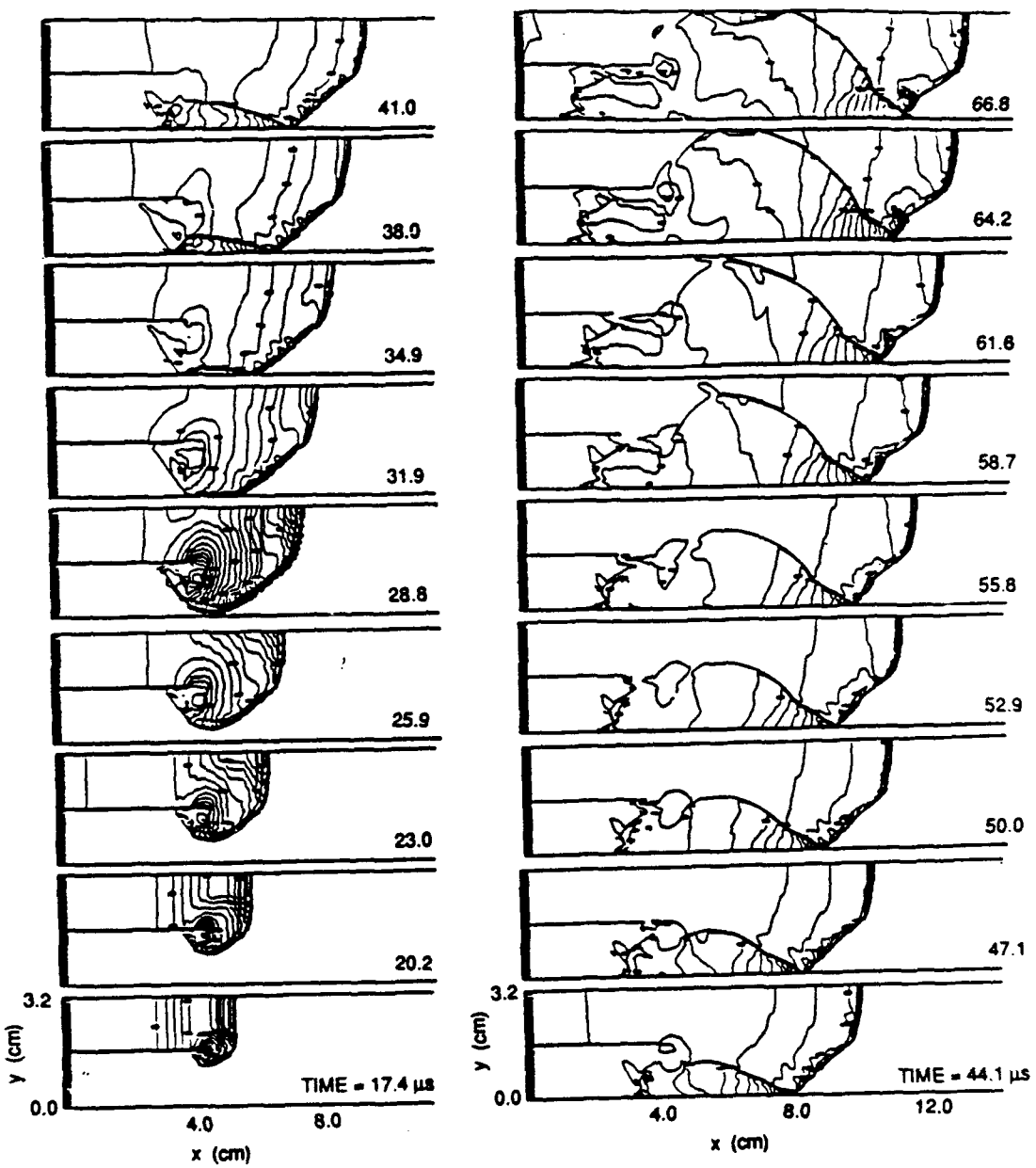

Figure 12. Simulated pressure contours for a detonation propagating in a stoichiometric, diluted primary mixture and a lean secondary mixture. Primary (upper) mixture H_2:O_2:Ar/2:1:7; secondary (lower) mixture H_2:O_2:Ar/0.5:1:7.

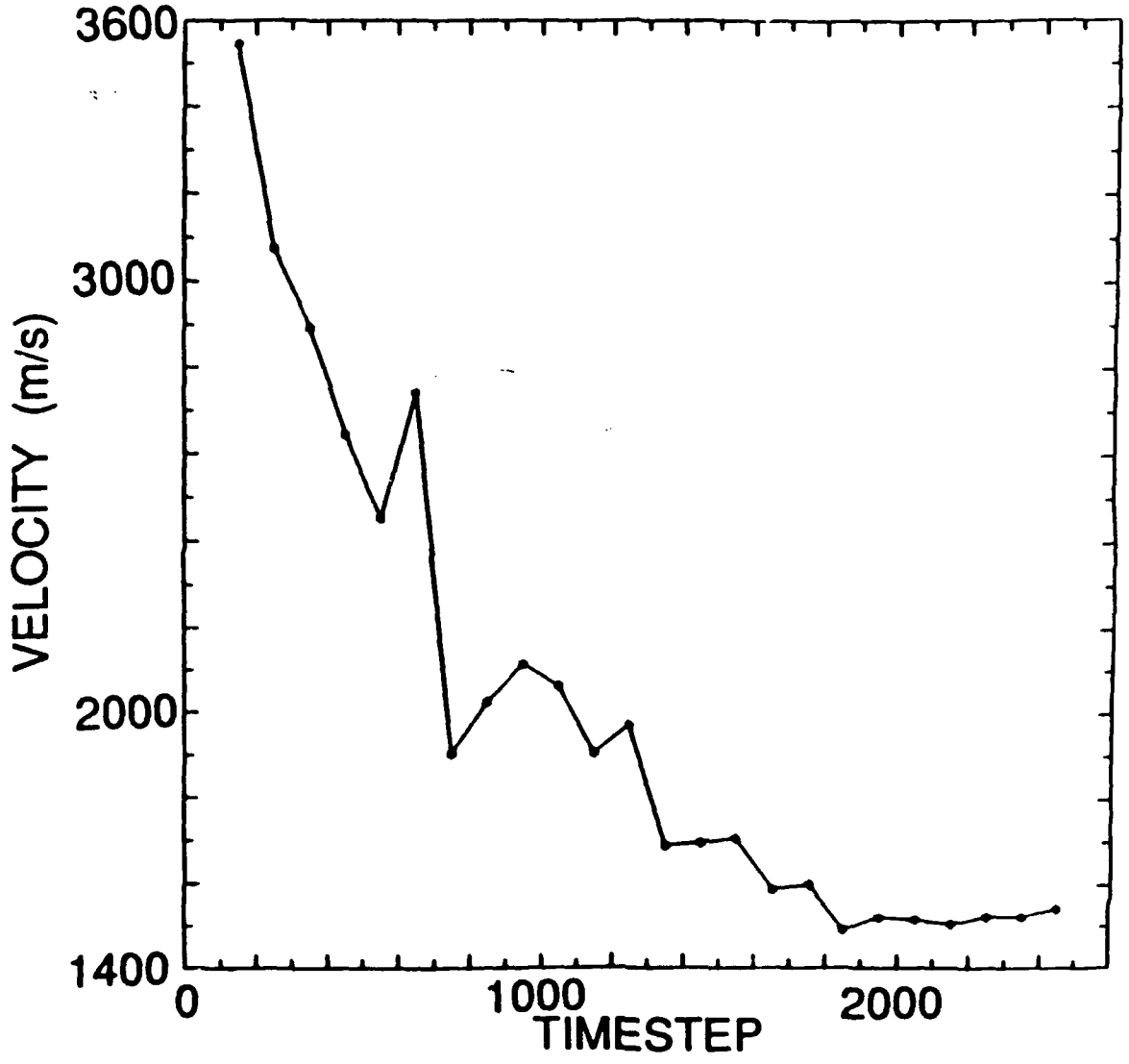

Figure 13. Velocity of the overdriven shock-detonation complex as a function of timestep for the computation shown in Figure 12.

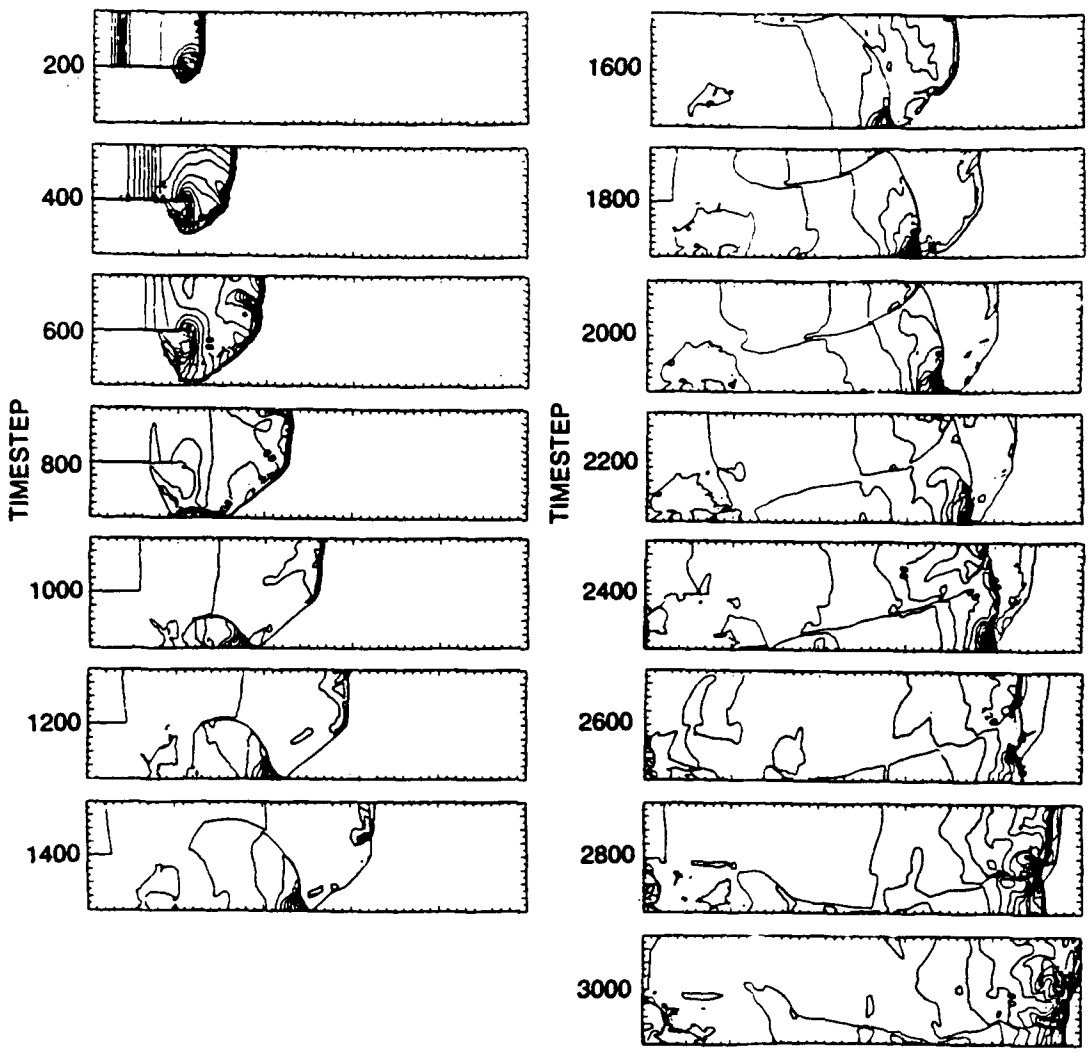

Figure 14. Pressure contours at selected timesteps for the primary CJ detonation in a diluted stoichiometric hydrogen-oxygen mixture into a lean mixture. The vertical height is 3.2 cm and the horizontal expanse is 20 cm. One timestep is approximately 5.0×10^{-8} seconds.

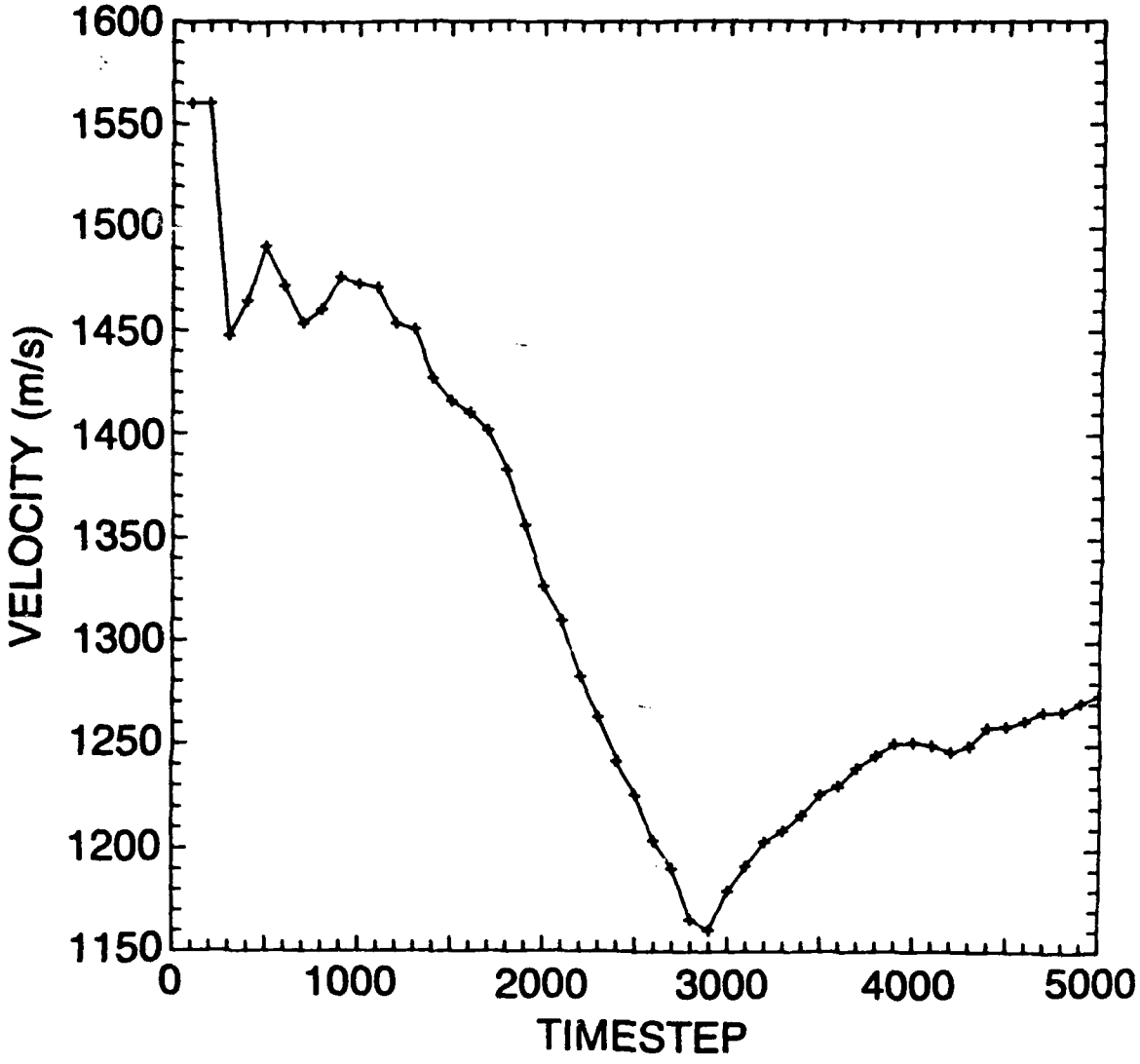

Figure 15. Velocity of the CJ shock-detonation complex as a function of timestep for the computation shown in Figure 14.

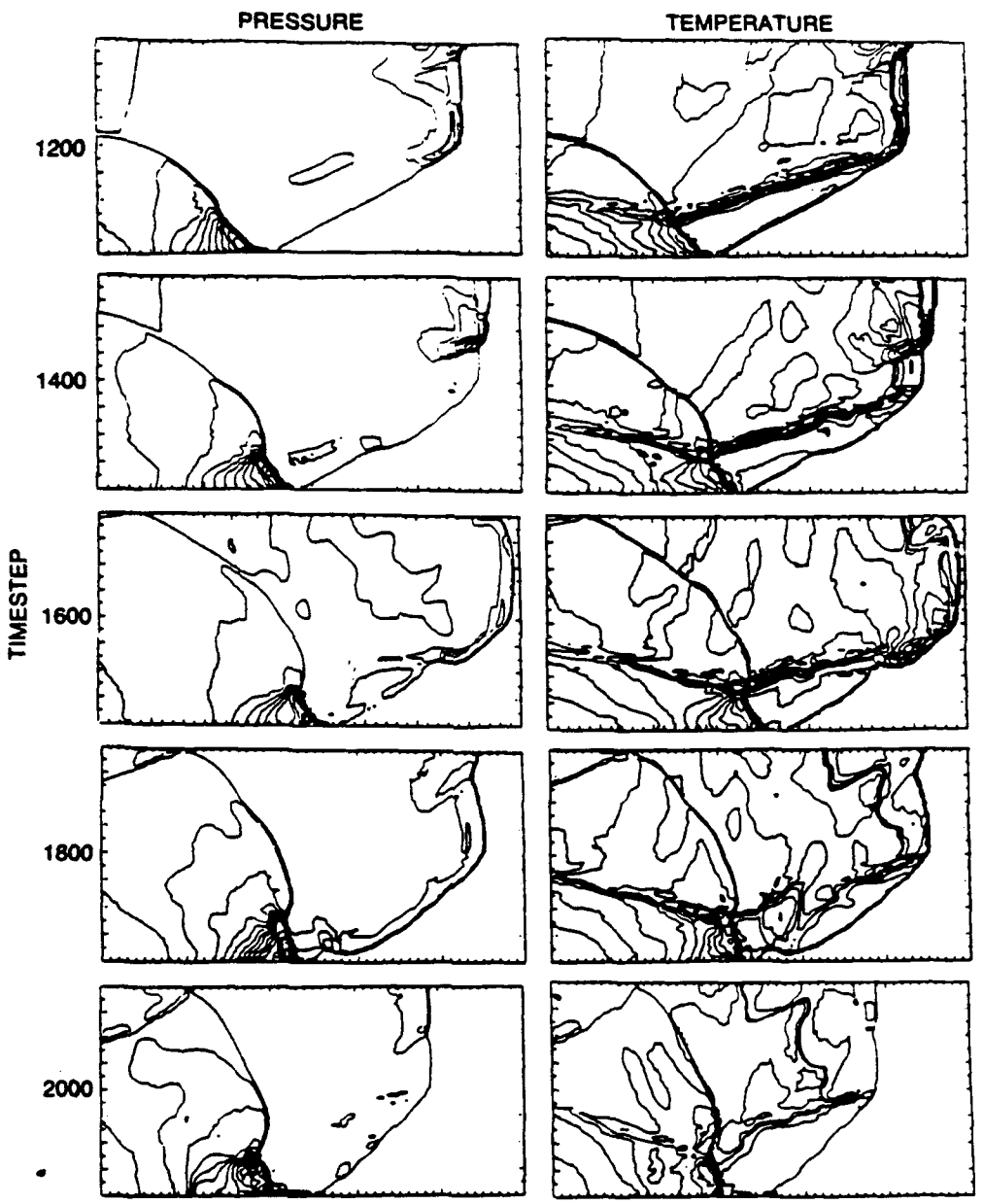

Figure 16. Pressure and temperature contours for steps 1200 to 2000, showing the decoupling of the shock and reaction wave in the primary detonation and possible reignition in the Mach stem in the lean mixture.

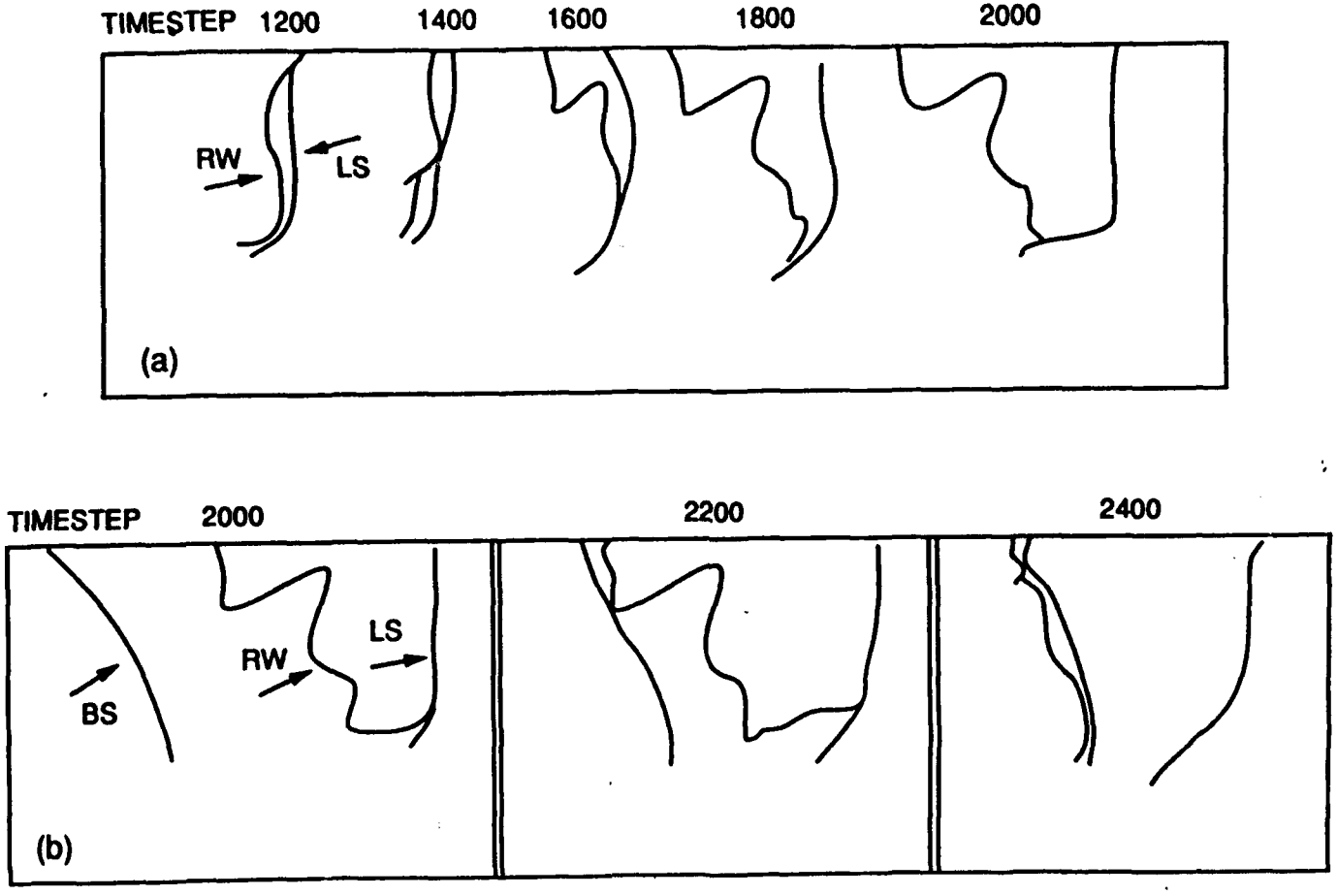

Figure 17. Tracings taken from pressure, temperature, and density contours in the upper tube showing a) the leading shock (LS) and reaction wave (RW) and b) the leading shock, reaction wave, and bubble shock (BS).

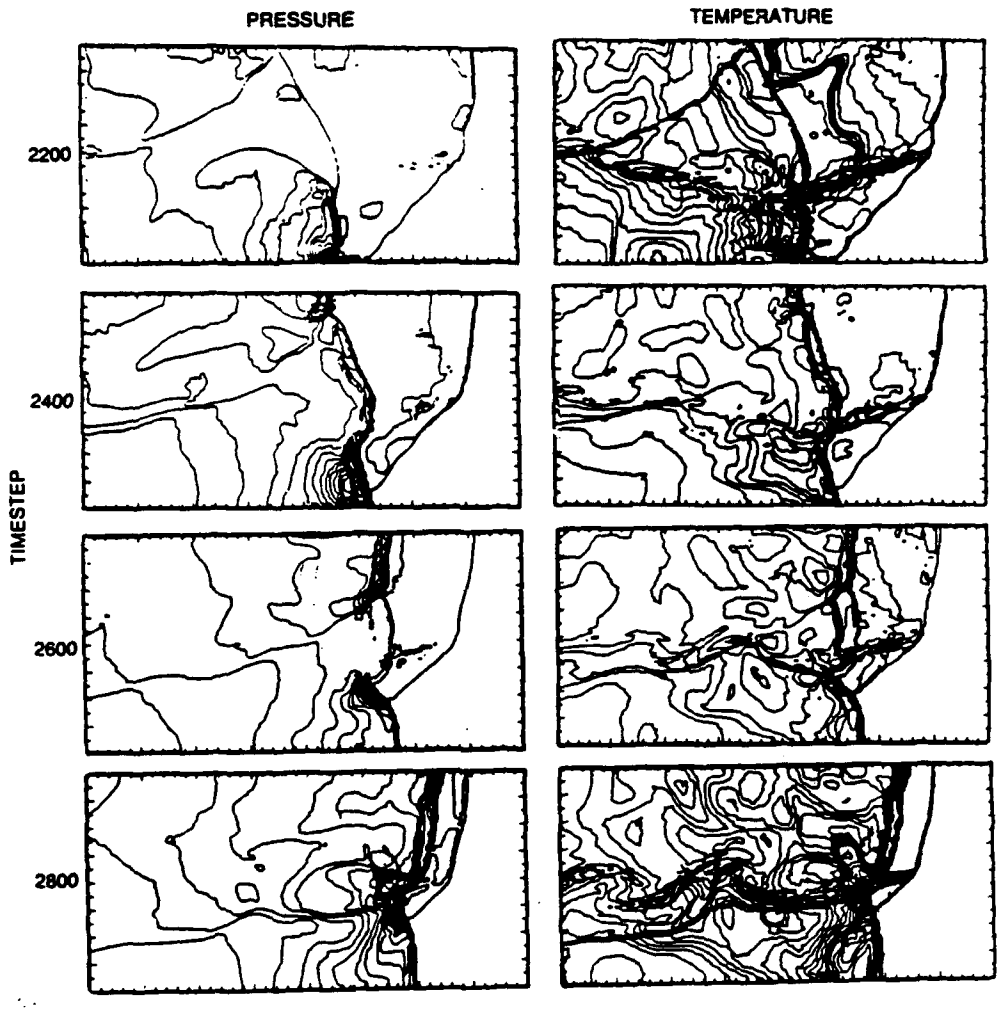

Figure 18. Pressure and temperature contours for steps 2200, 2400, 2600, and 2800 showing reignition in the primary and secondary mixtures.

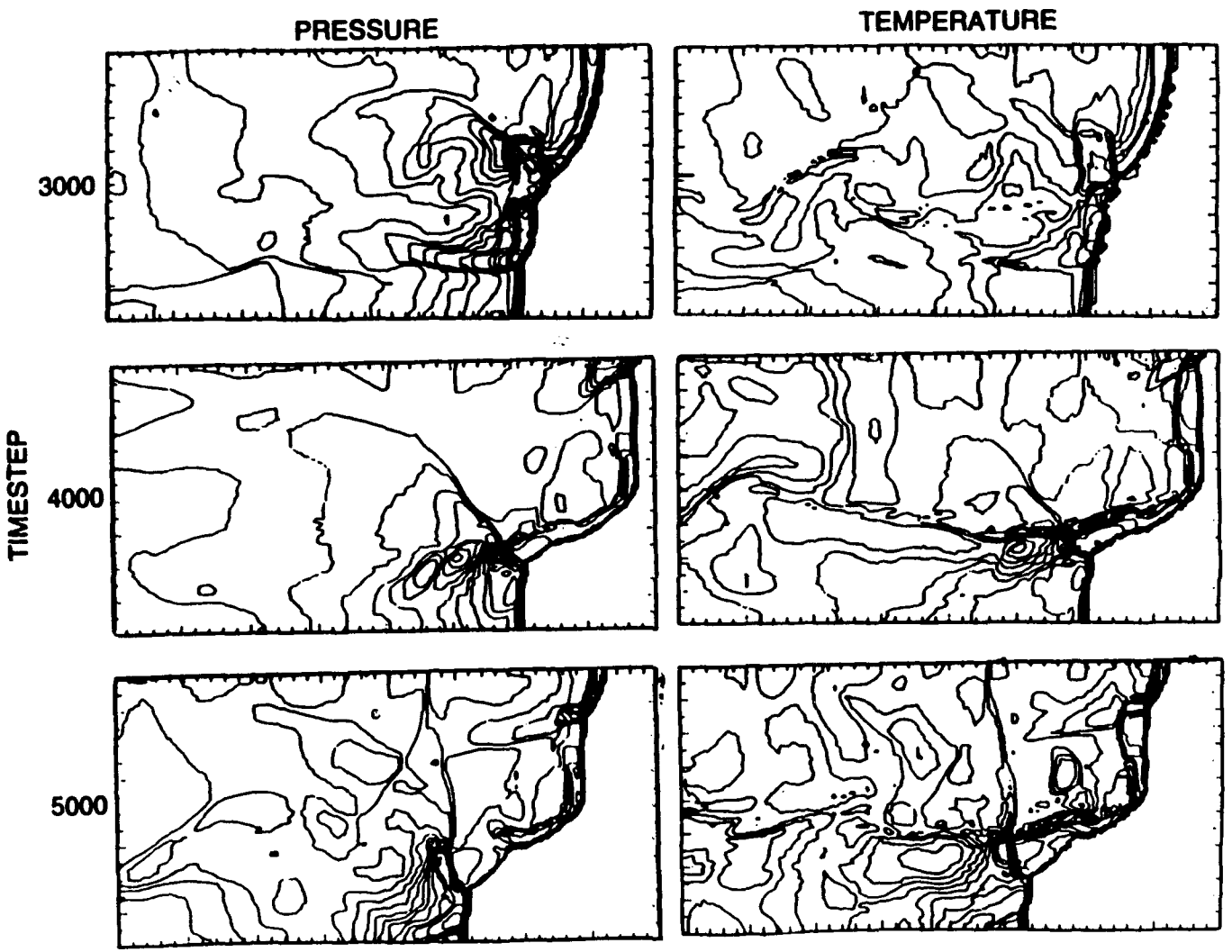

Figure 19. Pressure and temperature contours for late-time steps 3000, 4000, and 5000.